

The influence of shallow water on rock armour stability

Giulio Scaravaglione^a, Stefano Marino^b, Antonio Francone^a, Elisa Leone^a,
Leonardo Damiani^b, Giuseppe R. Tomasicchio^a, Marcel A. van Gent^c,
Alessandra Saponieri^{a*}

^aDepartment of Engineering for Innovation, University of Salento, Lecce, Italy;

^bDepartment of Civil, Environmental, Land, Building Engineering and Chemistry (DICATECh), Polytechnic University of Bari, Bari, Italy; ^cDepartment of Hydraulic Engineering, Delft University of Technology and Deltares, Delft, the Netherlands

* Corresponding author: Alessandra Saponieri

ABSTRACT

The hydraulic stability of rock armour layers has been extensively discussed in the literature, with numerous formulae proposed for design purposes. However, limited attention has been given to armour stability under shallow water conditions, largely due to the scarcity of experimental data. This research aims to address this gap by providing new insights into the stability of rock armour layers with rubble mound breakwaters in shallow water. Hydraulic stability was determined for four different structure slopes and various hydrodynamic conditions, spanning from deep to extremely shallow water in presence of a 1V:30H foreshore. Newly experimental data were compared with existing stability formulae valid in shallow water, specifically those by van Gent et al. (2003, VG), Eldrup and Andersen (2019, EA), and Etemad-Shahidi et al. (2020, ES). Initially, the data were used to evaluate the accuracy of the original formulae. Following this, the formulae were recalibrated to account for the influence of shallow water, with data grouped according to water levels. Finally, modified versions of VG and ES formulae were developed to fit the experimental data, incorporating the effects of wave steepness to better capture shallow water dynamics.

Keywords

Hydraulic stability, Rubble mound breakwater, Physical model tests, Damage, Shallow water.

1 **1. Introduction**

2 Rock-armoured rubble mound breakwaters are the most common coastal structures used
3 to protect harbours and mitigate coastal erosion and flooding. Although the estimation of
4 the hydraulic stability of the armour units is a standard practice for coastal engineers, this
5 calculation may be highly influenced by the stochastic nature of wave loading, movement
6 initiation, and armour damage progression (Campos et al., 2020a; 2020b). The formulae
7 reported in design manuals (e.g., Coastal Engineering Manual (USACE, 2002); Rock
8 Manual (CIRIA/CUR/CETMEF, 2007)) are semi-empirical and primarily based on
9 datasets from 2D physical model tests conducted worldwide.

10 Rubble mound breakwaters are commonly found along sandy coastlines, especially in
11 shallow water environments. The slopes characteristics of these sandy coasts can vary
12 significantly, ranging from gentle slopes, that allow waves to dissipate energy gradually,
13 to steeper slopes, such as 1V:20H or 1V:30H gradients. These steeper slopes influence
14 wave behaviour and the effectiveness of breakwaters, potentially requiring more robust
15 designs to ensure adequate coastal protection, as they are exposed to depth-limited waves,
16 significantly influenced by seabed. According to the water depth classification of van
17 Gent (1999, 2001), based on the ratio between the spectral wave height in deep water
18 ($H_{m0,o}$) and the water depth at the structure toe (h), namely the relative depth ($h_r = H_{m0,o}/h$),
19 different water depth conditions can be established, ranging from deep (where wave
20 breaking on the foreshore is absent) to extremely shallow foreshores (experiencing a high
21 degree of wave breaking on the foreshore). Specifically, foreshores can be classified as
22 deep ($h_r < 0.40$), intermediate ($0.40 < h_r < 0.75$), shallow ($0.75 < h_r < 1.50$), very shallow
23 ($1.50 < h_r < 3$), and extremely shallow ($h_r > 3$).

24 Shallow water represents a typical design condition for most coastal structures around the
25 world. They are, for example, prevalent along the U.S. (e.g., the Gulf of Mexico, Melby

26 et al., 2021) and the North Sea (e.g., the sea defence at Scarborough in the U.K., Allsop,
27 2021) for protecting harbours, navigation waterways, shorelines, and bluffs. Moreover,
28 hard-soft hybrid structures, such as dike-in-dune systems or large beach nourishments in
29 front of sea walls, can be found in the Netherlands and Belgium, where steep foreshores
30 represent a typical average (eroded) profile (Altomare et al., 2020). Such interventions
31 are characterised by large amounts of sand seaward of the hard structure (Altomare et al.,
32 2016), which can be eroded during extreme storms, potentially altering the water depth
33 conditions at the toe of the structure from intermediate/shallow to very/extremely
34 shallow. In these situations, the impact of wave forces on the structure is strongly
35 influenced by seabed topography and waves are completely different compared to deep
36 water (Allsop et al., 1999; Goda, 2010; Herrera and Medina, 2015). Shallow foreshores
37 are characterised by breaking waves and the release of bound long waves (van Gent,
38 2001). The energy spectrum tends to flatten and/or become double-peaked, resulting in a
39 prevalence of low frequency components in the surf zone, closely related to the incident
40 wave groups, which increase as waves approach the structure, leading to a reduction in
41 energy at higher frequencies (Kamphuis, 1996; Shah and Kamphuis, 1996).

42 Shallow water conditions are also expected to become more common with the upgrading
43 of existing breakwaters, driven by changing hydraulic conditions due to sea level rise. In
44 the context of probabilistic design, uncertainties in design conditions under climate
45 change require further research to fully understand wave-structure interaction phenomena
46 and their impact on the functionality of existing rubble mound breakwaters, since these
47 uncertainties could result in the breakwater being unable to meet the design requirements
48 (e.g., Calabrese et al., 2011; Ciardulli et al., 2013; Brancasi et al., 2022; Díaz-Carrasco
49 et al., 2023; Mares-Nasarre et al., 2024). Some possible solutions for upgrading damaged
50 rubble mound breakwaters should be selected based on clear adaptation pathways as

51 highlighted by van Gent and Teng (2023). Despite the practical relevance of upgrading
52 aging structures, limited research has been conducted on the subject (e.g., Burcharth et
53 al., 2014). Currently, no generic method exists to describe the rock armour stability in
54 extremely shallow water conditions, thus requiring a review and update of the current
55 state of knowledge and tools for slope breakwater design, especially in very and
56 extremely shallow water.

57 To this aim, new 2D experiments have been carried out in the wave flume at the European
58 Maritime and Environmental Research ([EUMER](#)) laboratory at the University of Salento
59 (Lecce, Italy) to investigate the effects of shallow water conditions on the hydraulic
60 stability of steep permeable rubble mound breakwaters.

61 The present paper is organised as follows: **Section 2** presents the literature background,
62 retracing the most relevant findings in rock armour stability over time. **Section 3**
63 describes the physical model setup and performed tests, including the experimental
64 programme and damage measurements. **Section 4** reports the wave analysis of the data
65 collected during the experiments. **Section 5** discusses the results and compares the new
66 experimental data with the available design formulae calibrated for shallow water
67 conditions (van Gent et al., 2003; Eldrup and Andersen, 2019; Etemad-Shahidi et al.,
68 2020). Additionally, modified versions of van Gent et al. (2003) and Etemad-Shahidi et
69 al. (2020) stability formulae for shallow water conditions are proposed to fit the
70 experimental data. Finally, **Section 6** provides a summary of the key findings of the
71 present study and presents perspectives for future research.

72 **2. Background**

73 Early relations describing the incipient motion of seaside armour stones were developed
74 by Iribarren (1938), Hudson (1959) and Losada and Gimenez-Curto (1979), in which the

75 relations differ primarily in the parametric description of the structure slope and friction
76 angle. The widely known Hudson formula has remained the most commonly used method
77 for many decades. At the end of the 1970s and beginning of the 1980s, catastrophic
78 failures were experienced by a series of large rubble mound breakwaters (Scaravaglione
79 et al., 2022), prompting extensive research to improve the design and construction of such
80 structures. Valuable results were achieved by Ahrens (1970), Ahrens and McCartney
81 (1975), and Thompson and Shuttler (1975). The last one recognised the importance of
82 factors as the type of wave breaking, rock placement, and the number of waves, thereby
83 generating a new dataset for flat bottom and impermeable slopes. Results of Thompson
84 and Shuttler (1975) were reanalysed by van der Meer (1988), who performed an extensive
85 laboratory experimental campaign, including both small- and large-scale tests, and
86 quantified the influence of further parameters, i.e., wave period, permeability, storm
87 duration and wave steepness. Based on his extensive dataset, van der Meer (1988)
88 proposed two different formulae for plunging and surging waves, widely employed in the
89 design practice, but mainly limited to deep water. Recently, van der Meer (2021) revisited
90 these equations, as shown in Eq. 1a,b:

$$N_s = \frac{H_s}{\Delta D_{n50}} = 6.49 c_{pl} P^{0.18} \left(\frac{S}{\sqrt{N_w}} \right)^{0.2} \xi_{s-1,0}^{-0.5} \quad \xi_{s-1,0} < \xi_{s-1,0,c} \quad \text{Eq. 1a}$$

$$N_s = \frac{H_s}{\Delta D_{n50}} = 0.97 c_{su} P^{-0.13} \left(\frac{S}{\sqrt{N_w}} \right)^{0.2} \cot \alpha^{0.5} \xi_{s-1,0}^P \quad \xi_{s-1,0} \geq \xi_{s-1,0,c} \quad \text{Eq. 1b}$$

91 where:

N_s	stability number
$H_s = H_{1/3}$	significant wave height in the time domain
$\Delta = \rho_r / \rho_w - 1$	relative buoyant density of the rock armour
ρ_r	density of the armour rock
ρ_w	density of the water
$D_{n50} = (M_{50} / \rho_r)^{1/3}$	armour nominal median rock size
M_{50}	median mass of the armour rock grading
α	structure seaward slope angle

$S=A_e/D_{n50}^2$	damage level
A_e	average eroded area (Broderick and Ahrens, 1982)
P	notional permeability factor
g	gravity acceleration
N_w	number of waves in a storm duration
$\xi_{s-1,0} = \tan \alpha / \sqrt{2\pi H_s / g T_{m-1,0}^2}$	surf similarity parameter
$T_{m-1,0}$	negative spectral energy wave period
$\xi_{s-1,0,c} = \left(\frac{6.49c_{pl}}{0.97c_{su}} P^{0.31} \sqrt{\tan \alpha} \right)^{\frac{1}{P+0.5}}$	critical surf similarity parameter
c_{pl}, c_{su}	coefficients that depend on the stone shape (Bradbury et al., 1988; Latham et al., 1988)

92 These formulae were calibrated using the datasets from Thompson and Shuttler (1975)
93 and van der Meer (1988) and are specifically valid in deep water for a non-sloping seabed.
94 For slopes more gentle than $\cot\alpha=4$, it is advised to use Eq. 1a, regardless of the value of
95 the surf-similarity parameter. Based on a limited number of tests with breaking waves on
96 the foreshore, van der Meer (1988) suggested replacing H_s with the wave height exceeded
97 by 2 percent of the waves that reach the breakwater ($H_{2\%}$), divided by the ratio $H_{2\%}/H_s=1.4$
98 valid for deep water conditions.

99 Later, Smith et al. (2002) conducted several small-scale laboratory tests to provide more
100 insights into shallow water conditions. This work was extended by van Gent et al. (2003)
101 to recalibrate the formulations proposed by van der Meer (1988), including conditions
102 with shallow foreshores (207 tests). By means of the datasets from van der Meer (1988)
103 and van Gent et al. (2003), modified equations for plunging (Eq. 2a) and surging (Eq. 2b)
104 waves were proposed:

$$\frac{H_s}{\Delta D_{n50}} = 8.4c_{pl}P^{0.18} \left(\frac{S}{\sqrt{N_w}} \right)^{0.2} \xi_{s-1,0}^{-0.5} \left(\frac{H_{2\%}}{H_s} \right)^{-1} \quad \xi_{s-1,0} < \xi_{s-1,0,c} \quad \text{Eq. 2a}$$

$$\frac{H_s}{\Delta D_{n50}} = 1.3c_{su}P^{-0.13} \left(\frac{S}{\sqrt{N_w}} \right)^{0.2} \cot\alpha^{0.5} \xi_{s-1,0}^P \left(\frac{H_{2\%}}{H_s} \right)^{-1} \quad \xi_{s-1,0} \geq \xi_{s-1,0,c} \quad \text{Eq. 2b}$$

105 where H_s and $T_{m-1,0}$ are both computed at the toe of the structure. For slopes more gentle
106 than $\cot\alpha=4$, it is advised to use Eq.2a, irrespective of the value of the surf-similarity
107 parameter.

108 Using the same database, van Gent et al. (2003) and van Gent (2004) reported an
109 alternative stability formula (Eq. 3), that does not depend neither on the spectral wave
110 period ($T_{m-1,0}$) nor the notional permeability factor (P), and includes the nominal rock
111 diameters of both the armour (D_{n50}) and core ($D_{n50,core}$):

$$\frac{H_s}{\Delta D_{n50}} = c_{VG} \sqrt{\cot\alpha} \left(1 + \frac{D_{n50,core}}{D_{n50}} \right) \left(\frac{S}{\sqrt{N_w}} \right)^{\frac{1}{5}} \quad \text{Eq. 3}$$

112 with $c_{VG}=1.75$.

113 Physical model tests conducted by Vidal et al., (2006), provided a new formula that
114 depends on the average of the 50 highest waves attacking the structure ($H_{1/50}$). In that
115 study the coefficients proposed by van der Meer (van der Meer, 1988) were recalibrated
116 to design breakwaters in intermediate and shallow water. Lamberti and Tomasicchio
117 (1997) also adopted $H_{1/50}$ to evaluate movement threshold conditions at reshaping berm
118 breakwaters. This approach allows for the consideration of extreme waves that could
119 affect breakwater stability, reducing the risk of damage during extreme storm events and
120 enhancing breakwater safety.

121 Melby and Hughes (2003) and Melby and Kobayashi (2011) proposed a stability formula
122 based on the maximum wave momentum flux, calibrated with the experimental data of
123 van der Meer (1988). These formulae are based on the physical assumption that wave
124 momentum flux at the toe of the structure is proportional to the maximum wave forces
125 on the armour units, showing that when the water depth is incorporated in the formulation,
126 a better description of stability is obtained.

127 Herrera et al. (2017) derived a new design formula in presence of breaking waves utilising
 128 a combined experimental-numerical approach with the SWAN numerical model (Booij
 129 et al., 1999) to compute the incident wave parameters inshore. The authors found that the
 130 best fit for their formula is obtained when the spectral wave height (H_{m0}) measured at
 131 three times the water depth far from the structure toe ($3h$) is used.
 132 Eldrup and Andersen (2019) investigated the hydraulic stability of a conventional rubble
 133 mound breakwater in shallow water, mainly focusing on the effects of nonlinear waves
 134 and very low wave steepness. They revisited the original van der Meer stability design
 135 formulae (van der Meer, 1988) and developed a new formulation (Eq. 4), based on the
 136 new acquired dataset (68 tests) and the ones provided by van Gent et al. (2003) and Eldrup
 137 et al. (2019):

$$\frac{H_{m0}}{\Delta D_{n50}} = c_{EA1} \left(\frac{S}{\sqrt{N_w}} \right)^{0.2} 1.6^P \xi_{m-1,0}^{(0.4P-0.67)} \quad \text{plunge with } \xi_{m-1,0} < \xi_{m-1,0,c} \quad \text{Eq. 4a}$$

$$\frac{H_{m0}}{\Delta D_{n50}} = c_{EA2} \left(\frac{S}{\sqrt{N_w}} \right)^{0.2} P^{0.17} \min[\cot\alpha, 2]^{0.23} \quad \text{surge with } \xi_{m-1,0} \geq \xi_{m-1,0,c} \quad \text{Eq. 4b}$$

138 where $s_{m-1,0} = 2\pi H_{m0} / gT_{m-1,0}^2$ is the wave steepness at the toe of the structure, $c_{EA1} = 4.5$,
 139 $c_{EA2} = 3.1$, and the critical surf similarity parameter ($\xi_{m-1,0,c}$) was redetermined (Eq. 4c):

$$\xi_{m-1,0,c} = \left(\frac{c_{EA2} P^{0.17} \min[\cot\alpha, 2]^{0.23}}{c_{EA1} 1.6^P} \right)^{\frac{1}{0.4P-0.67}} \quad \text{Eq. 4c}$$

140 By Eq. 4, a reduction in the uncertainty is achieved, indicating that H_{m0} may be preferable
 141 than $H_{1/3}$ or $H_{2\%}$ due to its lower sensitivity to wave nonlinearity.

142 In Etemad-Shahidi et al. (2020) a multi-variable regression model was used on the
 143 experimental database (791 data) available in literature (Thompson and Shuttler, 1975;
 144 van der Meer, 1988; van Gent et al., 2003; Vidal et al., 2006), to develop a compact

145 formula applicable across varying water depths for both plunging (Eq. 5a) and surging
 146 (Eq. 5b) waves:

$$\frac{H_s}{\Delta D_{n50}} = c_{ES1} C_p N_w^{-\frac{1}{10}} S_0^{\frac{1}{6}} \xi_{s-1,0}^{-\frac{7}{12}} (1-3m) \quad \text{for } \xi_{s-1,0} < 1.8 \quad \text{Eq. 5a}$$

$$\frac{H_s}{\Delta D_{n50}} = c_{ES2} C_p N_w^{-\frac{1}{10}} S_0^{\frac{1}{6}} \xi_{s-1,0}^{-\frac{1}{3}} (1-3m) \quad \text{for } \xi_{s-1,0} \geq 1.8 \quad \text{Eq. 5b}$$

147 where $C_p = \left[1 + \left(\frac{D_{n50,core}}{D_{n50}} \right)^{3/10} \right]^{3/5}$ represents the permeability coefficient, $c_{ES1}=4.5$ and
 148 $c_{ES2}=3.9$. These equations incorporate the effect of the foreshore slope (m) and are valid
 149 under depth-limited wave breaking conditions.

150 Losada (2021) questioned the classical methodology used to study the damage evolution
 151 of coastal slope structures and proposed a new predictive model, valid also in shallow
 152 water conditions, based on a sigmoid function. This approach aims to partially overcome
 153 the epistemic uncertainty inherent in the current damage evolution models, by
 154 considering the role of the relative depth and, particularly, the interplay between relative
 155 depth, wave steepness at the toe of the breakwater, and breakwater slope.

156 Despite various authors have derived different conclusions regarding the stability of rock
 157 armour in shallow water, data for very and extremely shallow water conditions (shallower
 158 than those tested or discussed in previous studies such as van Gent et al., 2003, Eldrup
 159 and Andersen, 2019 and Etemad-Shahidi et al., 2020) remains yet limited and scarce.
 160 Therefore, further research and physical model experiments are required to gain a deeper
 161 understanding of the effects of shallow water on rock armour stability.

162 **3. New laboratory tests**

163 **3.1 Physical model**

164 An experimental investigation was carried out in the wave flume at the EUMER

165 laboratory at the University of Salento (Italy). The wave flume is 45 m long, 2 m high,
166 and 1.4 m wide, equipped with a piston-type wave generator able to generate both regular
167 and second-order irregular waves characterised by target spectra shape (e.g., PM,
168 JONSWAP, TMA, double). The wave generator is equipped with an Active Reflection
169 Compensation system and a mild coarse and rocky spending beach ($\sim 1V:10H$) is placed
170 at the end of the flume to reduce as much as possible the re-reflection of the flume wall.
171 A 2D physical model of a rubble mound breakwater (**Figure 1**) was built with the toe
172 placed 29.10 m from the wave generator at the end of a 14.30 m long concrete foreshore
173 ($m=1V:30H$). The foreshore was connected to a flat bottom by means of a short 1.1 m
174 long transitional slope ($\sim 1V:5H$) ensuring sufficient depth at the wave generator. To
175 ensure proper wave shoaling and breaking along the foreshore and avoid the generation
176 of undesired nonlinear effects due to the presence of the transitional slope, the depth at
177 the end of the transitional slope (h_t in the range 0.59 m - 0.94 m) was ensured greater than
178 $0.025L_{p,o}$ (being $3.28 \text{ m} \leq L_{p,o} \leq 12.05 \text{ m}$), and the foreshore length greater than 3 local
179 wavelength along the foreshore (Frostick et al., 2011; Eldrup and Andersen, 2024).

180 During the experimental investigation, wave conditions along the flume were measured
181 through 8 resistive wave gauges (WG_i) with a sampling frequency equal to 40 Hz. Due
182 to the inherent limitations of reflection analysis in depth-limited conditions, all tests were
183 conducted with and without the structure to estimate the incident wave bulk parameters
184 at the toe of the breakwater. Indeed, two different layouts for wave gauges were used: (i)
185 for tests with the breakwater in the flume, and (ii) for wave calibration without the
186 breakwater. The wave gauges positions for both layouts are detailed in **Table 1**, providing
187 the absolute distance from the wavemaker.

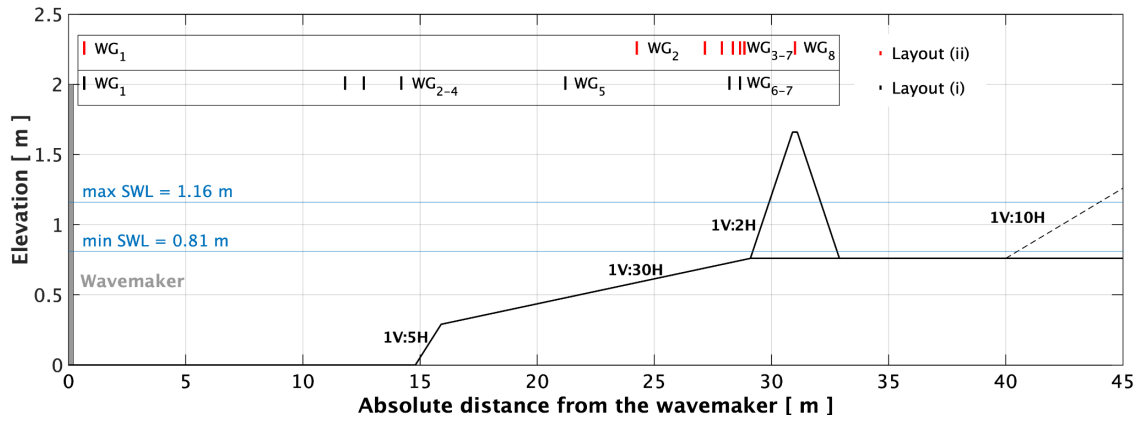
188 All the incident variables used in the further analyses refer to the incident wave
189 parameters measured at the WG_6 in layout (ii) (**Figure 1**), with no bandpass filter applied

190 to the acquired signals. The incident wave signals were obtained from the calibration tests
191 without the structure in place. This approach was chosen because most methods for
192 separating incident and reflected waves, particularly in the presence of sloping foreshores
193 and nonlinear waves (Lykke Andersen and Eldrup, 2024), fail to capture the true wave
194 behaviour. In fact, uncertainties in determining the incident wave parameters stem from
195 the nonlinear nature of waves, which, in shallow water, transform into breaking rollers.
196 It should be noted that, although the gauge WG6 is positioned relatively close to the toe,
197 the measured wave height may differ somewhat from the value directly at the toe, which
198 can be approximately 77% of the height recorded at WG6. These discrepancies arise from
199 the challenges of measuring waves in very shallow water depths, but they fall within the
200 typical uncertainties of physical modelling and are considered acceptable.

201 The measured free surface elevation from the calibration tests was used to calculate the
202 incident wave parameters, rather than relying on wave separation methods assuming the
203 good performance of the active absorption system. To verify the performance of the
204 absorption system, the measured wave spectra in deep water (WG1) were compared
205 against the target spectra provided by the wave generation system and with the incident
206 spectra obtained at the WG2-4 array with the model in place (layout (i)), showing
207 reasonable agreement.

208 The primary drawback of this approach is the introduction of errors caused by wave
209 reflection from the passive absorber during calibration tests. To account for the small but
210 existing reflection induced by the dissipative beach, the inshore bulk reflection
211 coefficient, K_R , was computed for all tests without breakwater in the flume
212 ($0.08 \leq K_R \leq 0.32$), using the method of Mansard and Funke (1980), as modified by Zelt and
213 Skjelbreia (1992), with a four-gauge-array among WG3-7 based on the optimal spacing
214 for the given water and wave conditions.

215 Since the total waves was measured at a distance of at least one wavelength from the
 216 dissipative beach, it was assumed that the incident and reflected waves were uncorrelated,
 217 allowing for the calculation of the incident wave height, as suggested by Goda (2000),
 218 using the formula $H_{m0,i}=H_{m0}/(1+K_R)^{1/2}$.



219 **Figure 1.** Cross-section of the physical model and wave gauges (WG_i) locations with
 220 (layout (i)) and without (layout (ii)) the breakwater in the flume.

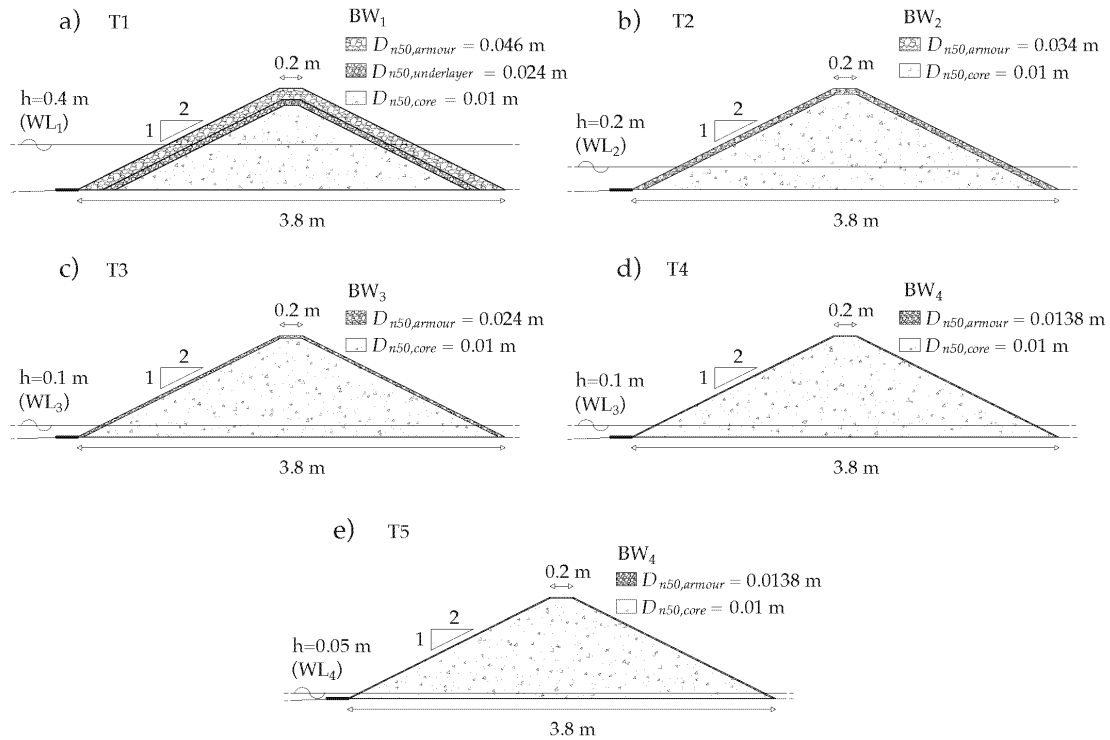
221 **Table 1.** Wave gauges absolute distance [m] from the wave generator.

Layout	WG ₁	WG ₂	WG ₃	WG ₄	WG ₅	WG ₆	WG ₇	WG ₈
(i)	0.66	11.8	12.6	13.2	21.2	28.20	28.65	-
(ii)	0.66	24.26	27.16	27.88	28.35	28.65	28.85	31.00

222 The structure was a conventional non-overtopped rubble mound breakwater without a toe
 223 berm. A small wooden slat, approximately 5 mm thick, was fixed seaward on the seabed
 224 near the toe, just in front of the bottom row armour rocks. Its purpose was to prevent the
 225 stones from sliding over the smooth surface during the tests, ensuring that wave forces
 226 acted primarily upslope, roughly 3 to 4 armour units from the toe. Very shallow water are
 227 the only scenarios where most of the wave energy is concentrated at the structure toe. In
 228 such cases, the presence of the wooden slat may slightly underestimate the observed
 229 damage. However, in real-world conditions, stones are likely to encounter resistance from
 230 accumulated sand, which is absent in the flume. Thus, these two factors effectively
 231 balance each other, aligning the lab results more closely with field conditions.

232 The breakwater was 0.9 m high with a 0.2 m wide crest. The dimensionless crest
233 freeboard ($R_c/H_{m0,t}$) above the still water level (SWL) was in the range of
234 $1.99 \leq R_c/H_{m0,t} \leq 21.79$, ensuring the avoidance of overtopping conditions. The breakwater
235 was protected by a double armour layer of rocks, randomly placed, with a front/rear slope
236 of $\alpha=1V:2H$. The armour layers consisted of natural rocks provided by a local quarry.
237 The placement of rocks can be considered bulk-random, and their shape can be assumed
238 as equant and fresh, according to the definition given by Latham et al. (1988). Therefore,
239 in the present work, it can be assumed that no significant differences occurred between
240 expected and predicted results, namely $c_{pl}=1.0$ and $c_{su}=1.0$ (van der Meer, 2021). The
241 thickness of the armour and filter layers were determined as $2D_{n50}$ and $0.5D_{n50}$,
242 respectively.

243 Four breakwater configurations (BW_i) and four water levels (WL_i) were tested across five
244 different test series (T_i), denoted as T1 (BW_1 and WL_1 , $h=0.40$ m), T2 (BW_2 and WL_2 ,
245 $h=0.20$ m), T3 (BW_3 and WL_3 , $h=0.10$ m), T4 (BW_4 and WL_3 , $h=0.10$ m), and T5 (BW_4
246 and WL_4 , $h=0.05$ m) (**Figure 2**). Notably, the structure with the highest water depth (T1)
247 was the only configuration with an underlayer composed by stones approximately half
248 the size of those in the armour layer, whereas the other structures consisted of an armour
249 layer atop the core material.

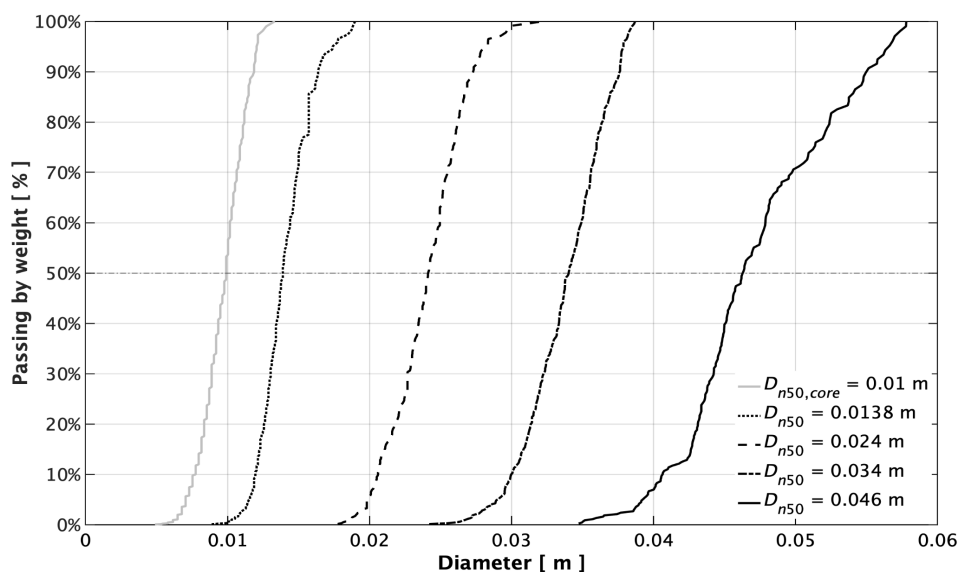


250 **Figure 2.** Layouts of the tested rubble mound breakwaters.

251 **Figure 3** and **Table 2** report, respectively, the sieving curves and the main characteristics
 252 of the rocks for each configuration, along with the notional permeability factor (P)
 253 calculated as proposed by Eldrup et al. (2019). Results show that the structure
 254 configuration BW_4 (**Figure 2d,e**) closely resembles a homogeneous structure ($P=0.55$),
 255 whereas the cross-sections with the lowest P -values (BW_1 and BW_2 in **Figure 2a,b**) are
 256 characterised by P -values close to 0.40, in line with the outcomes reported in van der
 257 Meer (1988).

258 **Table 2** also reports the $D_{n50,core}/D_{n50}$ ratio, the grading uniformity coefficient (D_{85}/D_{15}), the
 259 length-to-thickness ratio (LT), and the blockiness coefficient (BLC) used to assess the
 260 grading and the rough angular shape of rock in the armour layers for BW_1 , BW_2 and BW_3 ,
 261 following the procedures outlined in the Rock Manual (CIRIA/CUR/CETMEF, 2007).
 262 For the BW_4 configuration, the small dimensions of the stones did not permit conducting
 263 the same grading and shape characterisation as performed for the other configurations.
 264 These parameters were obtained by averaging the values from 20 samples randomly taken

265 from the grain population, as shown in **Figure 4**, where the standard deviation (std) for
 266 each sample population was also calculated.

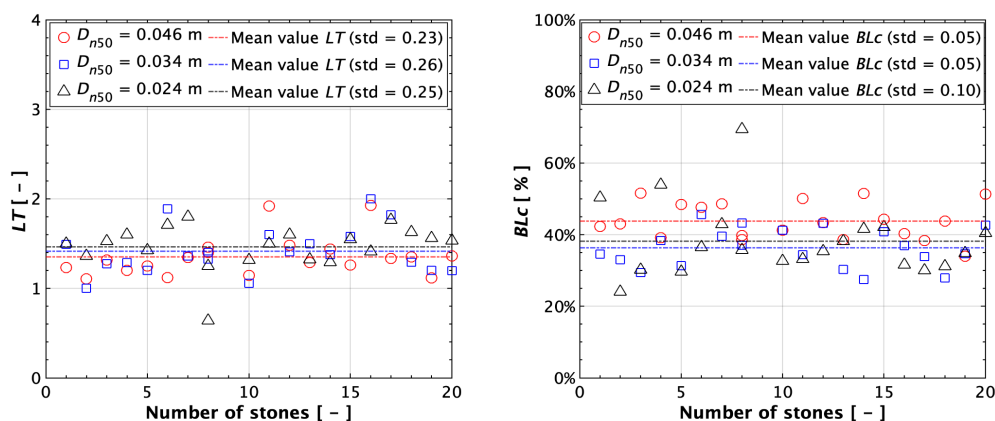


267 **Figure 3.** Rock sieving curves of the rock material used in the experiments.

268 **Table 2.** Main characteristics of rocks.

Breakwater configuration	BW ₁	BW ₂	BW ₃	BW ₄
D_{n50} [m]	0.046	0.034	0.024	0.0138
$D_{n50,underlayer}$ [m]	0.024	-	-	-
$D_{n50,core}$ [m]	0.01	0.01	0.01	0.01
$D_{n50,core}/D_{n50}$ [-]	0.21	0.29	0.41	0.71
D_{85}/D_{15} – armour [-]	1.26	1.27	1.20	1.28
LT – armour [-]	1.35	1.41	1.46	-
BLC – armour [%]	47.79	36.28	38.18	-
P -values [-]	0.37	0.40	0.47	0.55

269



270

271 **Figure 4.** Shape characterisation of the material used in the experimental campaign:
 272 length-to-thickness ratio (on the left) and blockiness coefficient (on the right).

273 The density of the stones was $\rho_r=2576 \text{ kg/m}^3$, and the porosity of the core (n) was assumed
274 equal to 0.40 (Rock Manual, 2007). In the present study, the Reynolds number was
275 calculated for both the armour layer (R_{eA}) and inside the porous core (R_{ep}) to assess the
276 flow regime inside the structure and the potential occurrence of scale effects (e.g., Wolters
277 et al., 2009, 2014; Scaravaglione et al., 2024). In intermediate and shallow water R_{eA}
278 exceeds 3×10^4 , and, hence, no scale effects are expected. In shallower conditions (i.e.,
279 T3, T4 and T5), R_{eA} results $0.75 \times 10^4 \leq R_{eA} \leq 2 \times 10^4$, indicating that some scale effects could
280 be present. Specifically, for T4 and T5, R_{eA} is slightly lower than 1×10^4 , and the test data
281 can be considered slightly conservative, meaning that the corresponding damage to the
282 prototype structure may be slightly less than those observed in the model tests (Hudson,
283 1975).

284 **3.2 Test programme**

285 A total of 33 tests were conducted to investigate the hydraulic stability of steep rock-
286 armoured rubble mound breakwaters. Experimental tests were grouped for each
287 configuration into two series, each one with increasing wave height and wave period at
288 the generator, while maintaining a constant target offshore spectral wave steepness (S_{m-}
289 $_{1,0,0}$) equal to 0.024 and 0.048, to simulate a storm with nonstationary conditions. After
290 each test, the structure was always rebuilt before the start of the subsequent test. For each
291 test, a minimum of 1000 waves were generated to examine the initiation and progression
292 of breakwater damage, employing a JONSWAP spectrum with an enhancement factor
293 $\gamma=3.3$. For some tests, damage was also measured after 3000 waves, as no significant
294 damage occurred after the initial 1000 waves. Tests were stopped before reaching 1000
295 waves when the underlayer (for T1) or the core (for T2, T3, T4, T5) became visibly
296 exposed to waves. In such cases, the reduced test duration (t_r) was used to correlate the

297 damage value with the exact number of incident waves, calculated as $N_w = t_r/T_m$, where T_m
 298 is the mean wave period in the time domain. In shallow water, since T_m near the toe of
 299 the breakwater may vary and directly impacts the wave count measurement, the N_w in
 300 deep water conditions ($T_{m,o}$) was considered. Before each test series, the rubble mound
 301 breakwater was exposed to a shake-down test characterised by low energy, to compact
 302 the armour rocks and settle the structure (Hughes, 1993).

303 The data obtained from these experiments encompass tests conducted under intermediate,
 304 shallow, very shallow, and extremely shallow water conditions, with and without wave
 305 breaking on the foreshore, including also surging and plunging breaking waves. The
 306 experimental investigation provided new stability data in very and extremely shallow
 307 water ($h_r > 1.5$). Specifically, among the 33 tests, 7 were performed in intermediate
 308 ($h = 0.40$ m), 10 in shallow ($h = 0.20$ m), 10 in very shallow ($h = 0.10$ m), and 6 in extremely
 309 shallow water ($h = 0.05$ m).

310 **Table 3** summarises the main characteristics of the experimental programme, including
 311 the number of tests for each breakwater configuration (N), the water depth at the
 312 breakwater toe (h), the relative depth (h_r), the measured offshore spectral wave steepness
 313 ($s_{m-1,0,o}$) and the measured stability number (N_s).

314 **Table 3.** Main characteristics of the performed tests.

Test ID	T1	T2	T3	T4	T5
Breakwater configuration	BW ₁	BW ₂	BW ₃	BW ₄	BW ₄
Water level	WL ₁	WL ₂	WL ₃	WL ₃	WL ₄
N [-]	7	10	6	4	6
h [m]	0.40	0.20	0.10	0.10	0.05
h_r [-]	0.42-0.75	0.71-1.40	1.49-2.54	1.49-2.03	2.98-4.94
$s_{m-1,0,o}$ [-]	0.024-0.051	0.025-0.047	0.024-0.046	0.024-0.046	0.024-0.046
$N_s = H_{m0,i}/AD_{n50}$ [-]	2.01-3.44	2.26-2.95	1.47-2.17	2.56-3.39	1.71-2.63

315 **3.3 Damage measurements**

316 Damage measurements were conducted using a high-density laser profiler provided by
317 HR Wallingford. Ten transects were sounded at intervals of 0.10 m across the width of
318 the flume. To avoid boundary-laboratory effects, clearances of 0.20 m and 0.30 m were
319 maintained from the left and right side walls of the wave flume, respectively. In the
320 analysis, the corner of the structure corresponds to the origin of the local reference system
321 ($x=0$, $y=0$, $z=0$), where the x -coordinate represents the longitudinal distance positively
322 towards the external side of the structure, the y -coordinate is the transversal direction
323 positively in the wave propagation direction, and the z -coordinate indicates the vertical
324 direction positively in the upper direction (**Figure 5a**). The laser profiler provides a
325 measurement resolution of ± 0.5 mm in both the y and z direction, with the same positional
326 accuracy guaranteed by the traverse laser support system (Atkinson and Baldock, 2016;
327 Marino et al., 2022, 2023).

328 The damage analysis followed similar procedures used by van der Meer (1988) and van
329 Gent et al. (2003), to ensure consistent and reliable comparisons among data derived from
330 different laboratory studies. Profiles were obtained before and after each test, referred to
331 as the mean initial (reference) and final profiles. As explained in **Section 3.2**, the damage
332 was measured after 1000 waves for almost all tests. When failure did not occur after 1000
333 waves, the test was continued up to 3000 waves (1000+2000), without reconstructing the
334 armour layer.

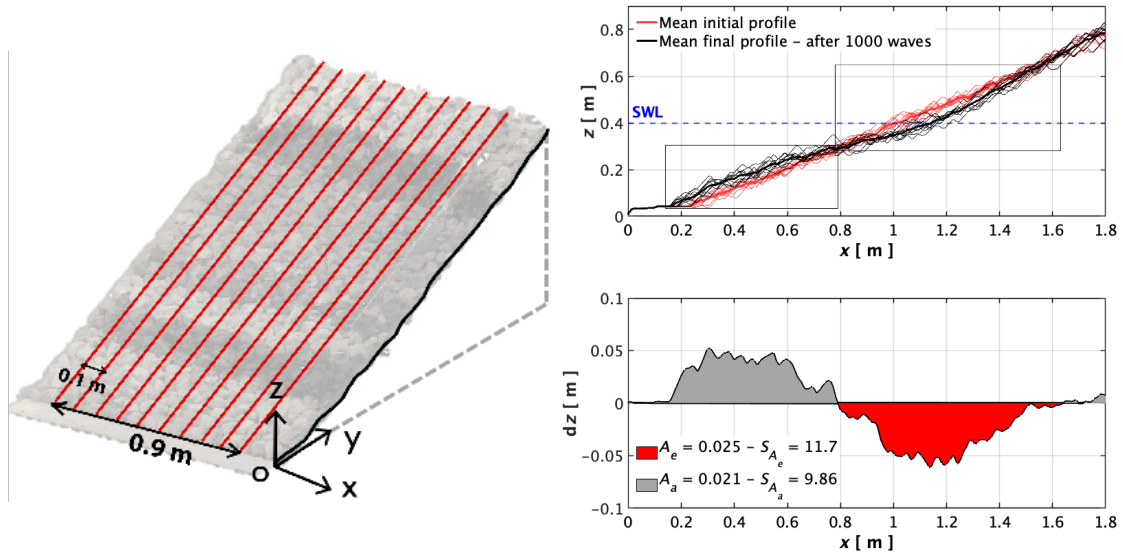
335 **Figure 5b** illustrates an example of reference and post-1000 wave profiles (test T1),
336 namely the initial and final mean elevation (z) relative to the local reference system ($z=0$),
337 averaged over the measured transversal transects. The eroded (A_e) and accretion (A_a) areas
338 were calculated as the integral function of the area under the negative and positive values
339 of the average spatial evolution of the slope (dz), also including minor displacements. The

340 damage level S was then estimated as A_e/D_{n50}^2 . **Table 4** reports the slope damage range
 341 measured during the experimental investigation for each test.

342 **Table 4.** Measured damage level ranges for each test series.

	T1	T2	T3	T4	T5
Slope damage: S [-]	1.8-20	1.4-11.05	1.3-3	9.6-18.4	1-8.21

343



344 **Figure 5.** On the left: Reference coordinate system and 10 transects across the flume
 345 width. On the right: Example of reference (red solid lines) and final (black solid lines)
 346 averaged profiles measured for the test T1 after 1000 waves (Top right). Spatial evolution
 347 of slope elevation changes (dz) with respect to the initial slope (Bottom right): erosion
 348 area (red) and accretion area (grey).

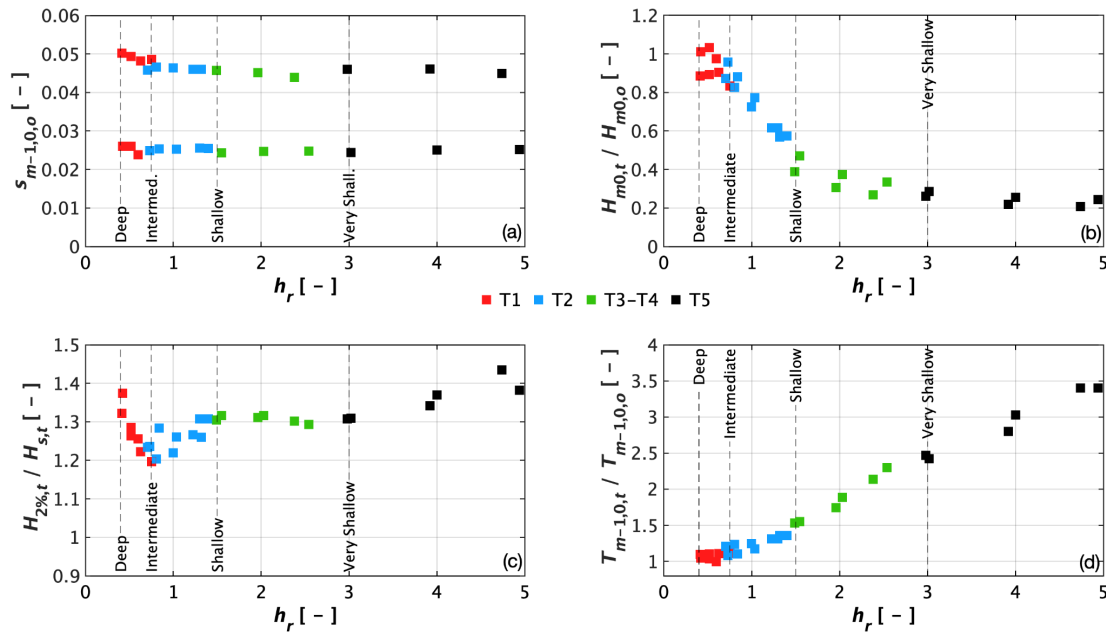
349 4. Wave analysis

350 The wave analysis was based on the time series of the incident waves recorded in front
 351 of the toe of the breakwater without the structure in the flume. **Table 5** reports the
 352 dimensionless parameters derived from the analyses and the range covered by the entire
 353 dataset. In **Figure 6** the measured offshore spectral wave steepness ($s_{m-1,0,o} = H_{m0,o}/L_{m-1,0,o}$),
 354 the relative wave height ($H_{m0,t}/H_{m0,o}$), the ratio $H_{2\%,t}/H_{s,t}$, and the relative wave period ($T_{m-1,0,t}/T_{m-1,0,o}$)
 355 are plotted against the relative depth (h_r) computed at the toe of the
 356 breakwater.

357 **Table 5.** Wave characteristics for each test series.

Main parameters	T1 (WL ₁)	T2 (WL ₂)	T3-T4 (WL ₃)	T5 (WL ₄)	Total
$H_{m0,o}/h$	0.42 – 0.75	0.71 – 1.40	1.49 – 2.54	2.98 – 4.94	0.42 – 4.94
$H_{2\%,t}/H_{s,t}$	1.20 – 1.37	1.20 – 1.31	1.29 – 1.32	1.31 – 1.43	1.20 – 1.43
$H_{m0,t}/H_{s,t}$	0.90 – 0.99	0.89 – 0.98	0.96 – 1.04	1.00 – 1.11	0.89 – 1.11
$T_{p,o}/T_{m-1,0,o}$	1.05 – 1.12	1.02 – 1.09	1.00 – 1.09	1.01 – 1.13	1.00 – 1.13
$H_{m0,t}/H_{m0,o}$	0.83 – 1.03	0.57 – 0.96	0.57 – 0.96	0.21 – 0.28	0.21 – 1.03
$T_{m-1,0,t}/T_{m-1,0,o}$	1.00 – 1.11	1.09 – 1.36	1.53 – 2.30	2.42 – 3.40	1.00 – 3.40

358



359 **Figure 6.** Wave characteristics as a function of the relative depth.

360 Previous data from van Gent et al. (2003) covers shallow and very shallow foreshore
361 conditions but does not include low steepness waves, whereas data from Eldrup and
362 Andersen (2019) supplements the van Gent et al. (2003) dataset, also covering smaller
363 wave steepness till to $s_{m-1,0,o}=0.01$. **Figure 6a** shows that new experimental data cover
364 real sea wave conditions (wind waves) in the range $0.02 < s_{m-1,0,o} < 0.05$, typically
365 considered in design scenarios. **Figure 6b** illustrates that two of the sea states experienced
366 a small amount of shoaling ($H_{m0,t}/H_{m0,o}$ slightly above 1) under relatively intermediate
367 conditions before reaching the structure toe, and hereafter, breaking is observed as the
368 relative depth decreases. In extremely shallow water conditions, the wave height
369 significantly decays up to 20% of the offshore spectral one. Tests involving low steepness

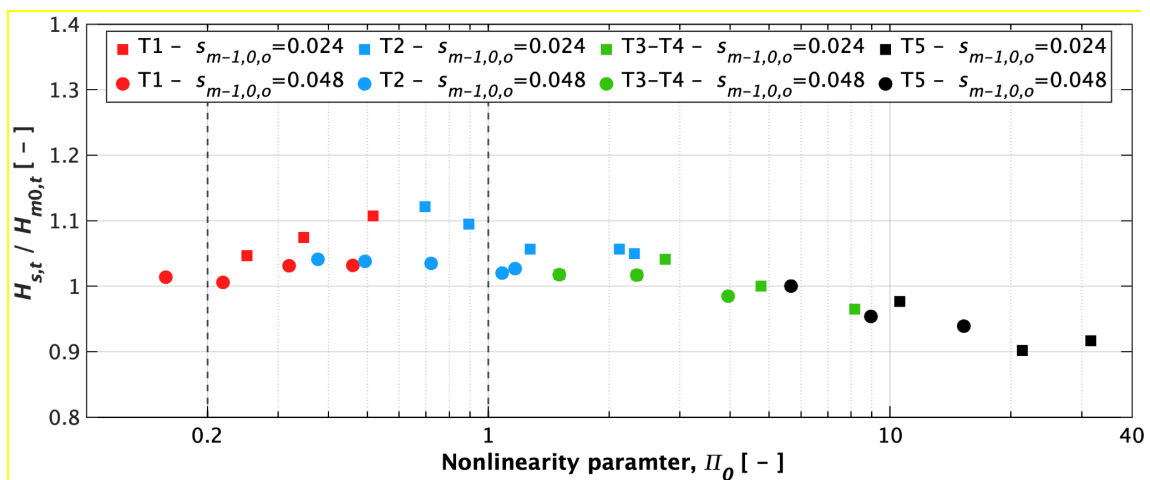
370 waves in shallow foreshore exhibit high nonlinearity and shoaling processes in
371 intermediate water conditions, whereas the others break due to a large wave steepness.

372 **Figure 6c** shows that in deep waters, where wave breaking is absent, wave heights can
373 be assumed to be Rayleigh distributed, and the ratio $H_{2\%,t}/H_{s,t}$ tends to 1.40. As waves
374 propagate and shoal towards the shore, nonlinear shoaling process enhances individual
375 wave heights, leading to a deviation in the wave height distribution from the expected
376 Rayleigh distribution. After waves enter the surf zone, the random wave breaking process
377 strongly modifies the wave height distribution. The ratio, indeed, decreases from 1.4
378 down to 1.2 in shallow water ($h_r > 0.75$), where the ratio begins to increase again and tends
379 to stabilise at very shallow water around 1.3, increasing once more in extremely shallow
380 water ($h_r > 3$) up to 1.40. Consistently with the findings reported by Goda (2010, 2012),
381 the wave height distribution returns to follow the Rayleigh one as waves approach the
382 shoreline.

383 The trend of the relative wave period ($T_{m-1,0,t}/T_{m-1,0,o}$) against the relative depth is depicted
384 in **Figure 6d**. Infragravity (IG) waves in the wave flume are likely to significantly
385 influence wave parameters, especially $T_{m-1,0,t}$. As waves propagate along the flume, the
386 spectral wave period at the toe increases, reaching nearly four times the deep water period
387 under extremely shallow conditions, due to wave transformation along the foreshore
388 (Hofland et al., 2017). This means that almost all the energy in the proximity of the peak
389 of the spectra is dissipated due to wave breaking at the same time as IG energy is increased
390 and such a behaviour is more pronounced as the relative depth increases, particularly in
391 very and extremely shallow conditions.

392 **Figure 7** reports the ratio $H_{s,t}/H_{m0,t}$ plotted against the nonlinearity parameter for all tests,
393 corresponding to the two target deep wave steepness values. Goda (2010) described the

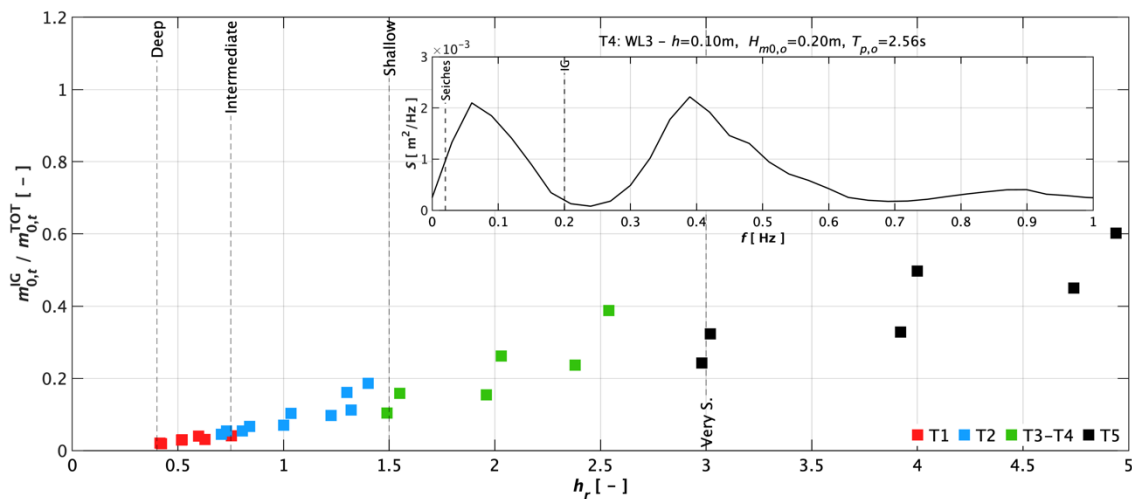
394 nonlinearity parameter as $\Pi_0 = \frac{H_{m0,o}}{L_{m,o}} \coth\left(\frac{2\pi h}{L_{m,o}}\right)^3$, where $L_{m,o}$ is the local wavelength
 395 calculated with T_m . For $\Pi_0 \leq 0.2$, data show that the ratio $H_{s,t}/H_{m0,t}$ is approximately 1, but
 396 a clear difference is observed in the range $0.2 < \Pi_0 < 1$, where $H_{s,t}/H_{m0,t}$ increases, reflecting
 397 the expected mean behaviour for low steepness waves according to Goda (2010). For
 398 $\Pi_0 \geq 1$, the ratio decreases to around 0.9. In relatively shallow water wave nonlinearity
 399 increases with an increase in wave height. As waves approach the shore, they undergo
 400 nonlinear shoaling, resulting in wave profiles with high and sharp crests and low and flat
 401 troughs. This nonlinearity effect becomes most pronounced around the outer edge of the
 402 surf zone. Within the surf zone, waves begin to break, and nonlinearities are gradually
 403 lessened, in accordance with wave steepness. Specifically, low steepness waves
 404 experience significant nonlinear shoaling before breaking, whereas high steepness waves
 405 break earlier.



406
 407 **Figure 7.** Wave height ratio as a function of the nonlinearity parameter.

408 **Figure 8** provides further insights into the energy spectral spreading during wave
 409 propagation in shallow water by showing the ratio $m^{IG}_{0,t}/m^{TOT}_{0,t}$ at varying relative depth,
 410 where $m^{IG}_{0,t}$ represents the infragravity (IG) wave energy component, and $m^{TOT}_{0,t}$
 411 represents the total wave energy, both evaluated at the structure toe. The inset plot shows
 412 an example of the density spectrum for a test in very shallow water (T4), evaluated at the

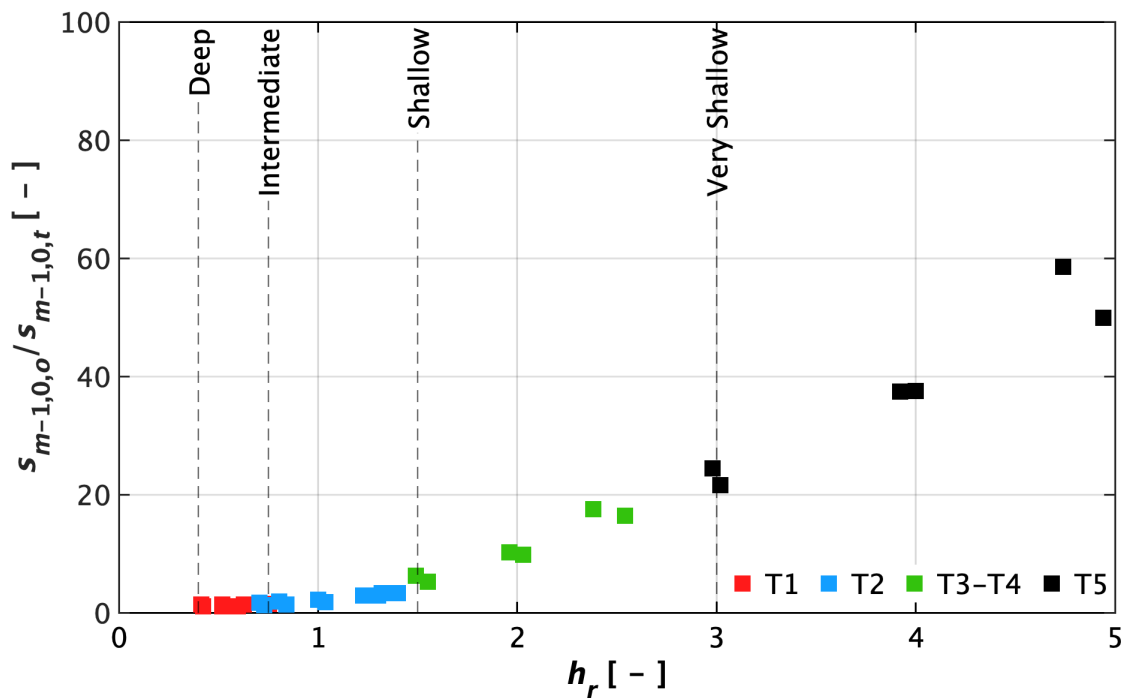
413 toe, highlighting the dominant peak frequencies. As water depth decreases, wave breaking
 414 begins, causing dissipation of energy at the peak and higher harmonic frequencies, while
 415 energy at lower frequencies continues to increase. Due to the very long wavelengths of
 416 these low-frequency waves, they do not break, and the substantial energy present at these
 417 lower frequencies explains the observation of large wave periods in shallow water. The
 418 spectrum clearly indicates significant energy in the infragravity frequency band in very
 419 shallow water. Results, indeed, demonstrate that, in the deep water, the infragravity waves
 420 minimally contribute to the total wave energy, but this contribution becomes
 421 progressively more significant as the water depth decreases. The most noticeable increase
 422 in the ratio occurs in extremely shallow water, where $m_{0,t}^{IG}/m_{0,t}^{TOT}$ values are the highest
 423 and the energy of IG components reach also the 60% of the total wave energy.



424 **Figure 8.** Ratio $m_{0,t}^{IG}/m_{0,t}^{TOT}$ as a function of the relative depth. The inset plot reports an
 425 example of the energy density spectrum for T4, at the wave gauge WG6.
 426

427 In **Figure 9** the spectral wave steepness computed at the toe of the structure is reported
 428 as a function of the relative depth (h_r). It was computed using $H_{m0,t}$ and $L_{m-1,0,t}$, where $L_{m-1,0,t}$
 429 $_{1,0,t}$ was calculated using the deep water wavelength formula, with the spectral wave
 430 period at the toe ($T_{m-1,0,t}$). Since the spectral shape changes significantly in extremely
 431 shallow water the wave steepness becomes very low. The increased energy at lower
 432 frequencies results in an exceptionally large spectral wave period. However, it is

433 important to emphasise that the total wave steepness is dominated by the energy at the
 434 lower frequencies making it less representative of the wave field and the steepness of the
 435 short waves. As expected, the wave steepness ratio ($s_{m-1,0,o}/s_{m-1,0,t}$) increases from
 436 intermediate to extremely shallow water conditions. However, it should be noted that in
 437 such conditions, waves break over a wide surf zone on the foreshore and not directly on
 438 the structure slope.



439 **Figure 9.** Influence of the relative depth on $s_{m-1,0,o}/s_{m-1,0,t}$ for different shallowness
 440 conditions.

441 In **Table 7**, the datasets utilised for the calibration of the stability formulae compared
 442 with the new experimental data (van Gent et al., 2003; Eldrup and Andersen, 2019;
 443 Etemad-Shahidi et al., 2020), are reported together with the range of the main parameters
 444 explored in this experimental investigation. Specifically, the new dataset covers ranges
 445 of the relative water depth at the structure toe (h_r) from 0.42 to approximately 5, extending
 446 the previous range of investigation.

447

448 **Table 7.** Range of parameters used for calibrating design formulae.

Rock stability formulae valid in shallow water conditions				
	Van Gent et al. (2003)	Eldrup and Andersen (2019)	Etemad Shahidi et al. (2020)	Present study
Datasets used for stability formulae calibration	Van der Meer (1988) Van Gent et al. (2003)	Van Gent et al. (2003) Eldrup et al. (2019) Eldrup and Andersen (2019)	Van der Meer (1988) Thompson and Shuttler (1975) Van Gent et al. (2003) Vidal et al. (2006)	EUMER
Parameters				
Structure slope angle: $cot\alpha$	1.5 - 6	1.5 - 4	1.5 - 6	2
Foreshore slope angle: $cotm$	Flat, 30, 100	30, 100	Flat, 30, 100	30
D_{n50} [m]	0.022 - 0.21	0.022 - 0.044	0.0164 - 0.21	0.0138 - 0.046
$D_{n50,core}/D_{n50}$	0.0 - 1.0	0.0 - 0.45	0.0 - 1.0	0.21 - 0.71
Relative mass density: Δ	0.90 - 2.05	1.62 - 1.75	0.92 - 2.05	1.576
Notional permeability: P	0.10 - 0.60	0.10 - 0.50	0.1 - 0.6	0.37 - 0.55
Offshore wave steepness: $S_{m,o}$	0.004 - 0.064	0.009 - 0.063	0.004 - 0.081	0.020 - 0.049
Offshore surf similarity parameter: $\xi_{m,o}$	0.67 - 7.58	1 - 6.77	0.67 - 7.58	2.26 - 3.54
Relative depth at the structure toe: h_r	0.058 - 1.5	0.18 - 1.5	0.038 - 1.5	0.42 - 4.94
Stability number: N_s	0.7 - 4.38	0.7 - 4.27	0.7 - 4.38	1.47 - 3.44
Slope damage: S	< 62	< 62	< 62	1.01 - 20.03
Number of waves: N_w	< 3000	492 - 5172	492 - 5172	652 - 4064
Number of data: N	579 + 207	207 + 68	791	55

450 **5. Results**

451 **5.1 Damage analysis**

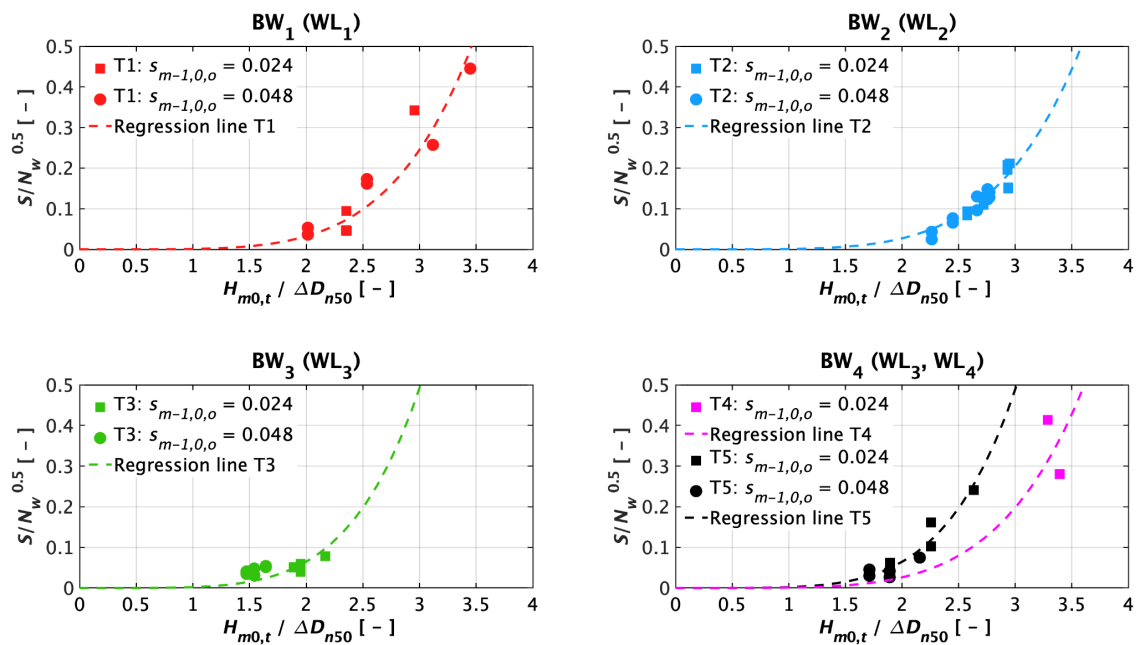
452 The relationship between damage values (S) and stability numbers (N_s) computed at the
453 toe of the breakwater is typically represented by a power relationship (Eq. 6):

$$S=a(N_s)^b \qquad \text{Eq. 6}$$

454 where ‘ a ’ and ‘ b ’ are regression coefficients calibrated using measured values through
455 the nonlinear least squares method. Specifically, the coefficient b defines the shape of the
456 damage curve and has been recognised as the reference coefficient for comparing damage
457 curves from different datasets. Van der Meer (2021) has underlined that a proper
458 comparison among damage results from different experimental investigations is possible
459 if the exponents of the damage curves are comparable. Hence, in the present work, the
460 same methodology described by van der Meer (1988) was replicated to derive the
461 coefficient of the damage fitting curve from the new experimental data. Overall, the
462 exponent ‘ b ’ was found to fall within the range $4.09 \leq b \leq 5.07$, yielding shape factors for
463 the damage curve ranging from $S=f(N_s^4)$ to $S=f(N_s^5)$ similar to previous studies, where
464 $b=5$ was found. In the analyses, S -values in the range $1 \leq S \leq 15$ were considered, as larger
465 values fall outside the range of practical relevance. Accordingly, in **Figure 10** the
466 experimental damage curves are plotted against the stability number for both deep target
467 steepness along with the 5-power regression line (dotted curve) for each breakwater
468 configuration (BW_i). Results show that, as expected, in all tests the damage increases as
469 the stability number increases and no evident differences can be observed between the
470 two wave steepness values. For the BW_4 configuration tested at two different water levels
471 (WL_3 and WL_4), it was observed that, despite the same structure configuration, the
472 stability behaviour varied under different water level conditions likely because different

473 wave steepness do not follow the same stability curve in deep water, and therefore it is
474 not expected they would in shallow water either.

475 The following subsections present the analyses on the influence of shallow water
476 conditions on the stability of a rock-armoured steep breakwater. This is achieved by
477 evaluating the accuracy of the formulae developed by van Gent et al. (2003) (VG, Eq. 3),
478 Eldrup and Andersen (2019) (EA, Eqs. 4a and 4b), and Etemad-Shahidi et al. (2020) (ES,
479 Eqs. 5a and 5b) against newly acquired experimental data. First, the accuracy of the
480 original formulae is assessed relative to this new data. Then, the formulae are recalibrated
481 to account for shallow water conditions, with the data categorised by water levels and
482 new regression coefficients calculated. Modified versions of the VG and ES formulas are
483 also explored to fit the new experimental data and are specifically valid for the range of
484 application investigated here, incorporating the incident wave steepness to better capture
485 the effects of shallow water.



486 **Figure 10.** Slope armour damage S against the stability number $N_s = H_{m0,t} / \Delta D_{n50}$.

487

5.2 Comparison with existing formulae valid in shallow water

488

5.2.1 Van Gent et al. (2003)

489

490

491

492

493

494

495

496

497

498

499

500

501

502

503

504

505

506

507

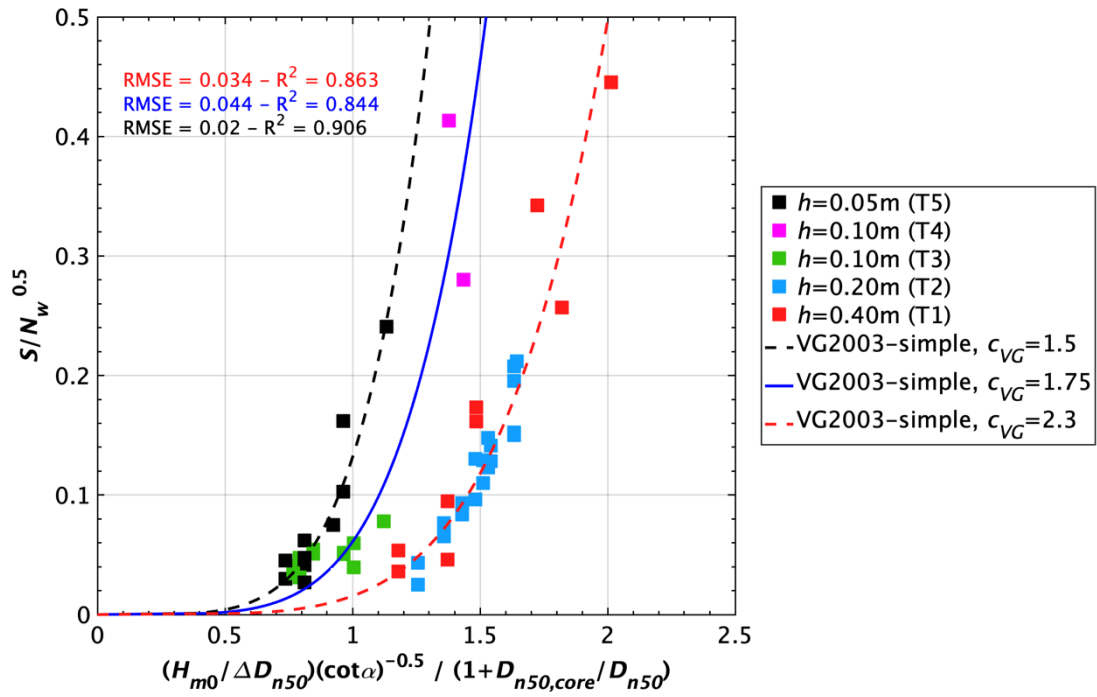
508

509

510

511

Figure 11 reports the observed dimensionless damage according to the VG expression (Eq. 3), with the experimental data aggregated into 4 groups based on the investigated water levels: intermediate (red squares, $h=0.40$ m), shallow (blue squares, $h=0.20$ m), very shallow (green and magenta squares, $h=0.10$ m), and extremely shallow (black squares, $h=0.05$ m) water. The theoretical curve (blue line, with $c_{VG}=1.75$) derived from Eq. 3 is also plotted. With respect to the theoretical regression line, a good prediction of damage is observed for very shallow water (tests T3 and T4) in both breakwater configurations (BW₃ and BW₄) at the same water level, regardless of the permeability. However, an overestimation of the predicted damage for intermediate/shallow water (tests T1 and T2), and an underestimation of damage for extremely shallow water (test T5) are observed. Therefore, for each water level, the formula was refitted to derive a new regression coefficient c_{VG} , to better fit the experimental data. In these analyses, the time-domain significant wave height (H_s) is replaced with the significant spectral one (H_{m0}) to minimise the influence of spectral shape and wave nonlinearity effects compared to low exceedance time domain wave heights (e.g., H_s or $H_{2\%}$). Moreover, frequency-based parameters (H_{m0} and $T_{m-1,0}$) are commonly used in practical design and typically derived from numerical wave models, making them readily available without relying on empirical relations, unlike time domain parameters that necessitate detailed knowledge of the wave height distribution. Results show that data in intermediate ($h=0.40$ m) and shallow ($h=0.20$ m) water exhibit similar behaviour (red dotted line, $c_{VG}=2.3$) and can be clustered, whereas data in extremely shallow water ($h=0.05$ m) are well represented by Eq. 3 if a regression coefficient c_{VG} equal to 1.5 is used (black dotted line).



512 **Figure 11.** Refitting of the van Gent et al. (2003) formula with the new data.

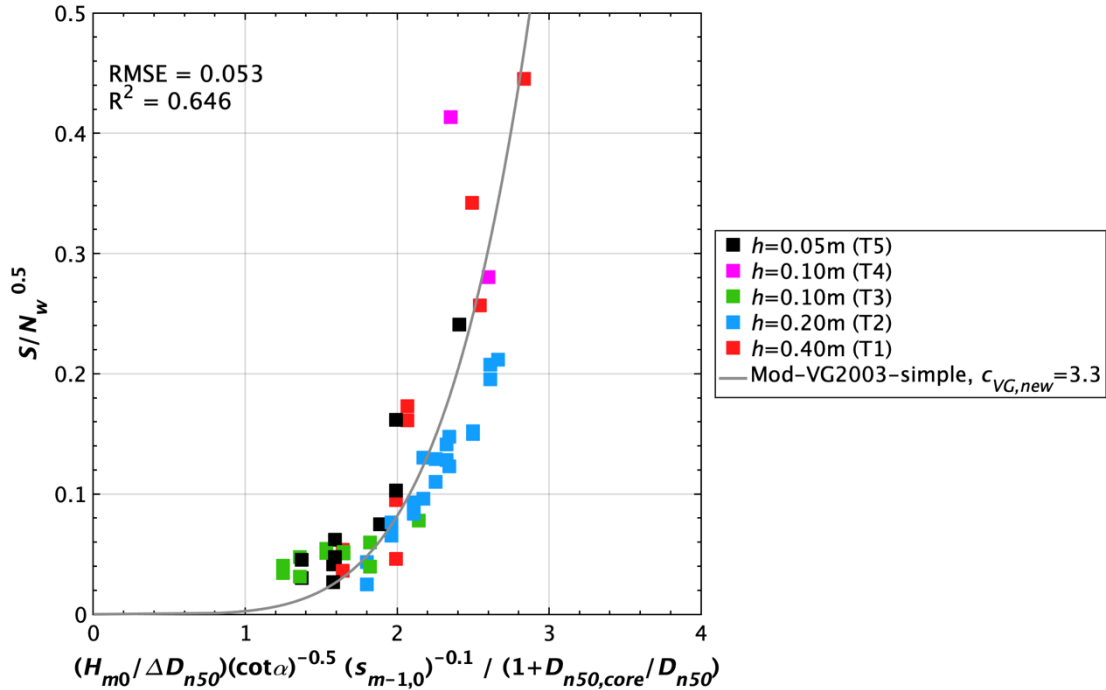
513 From these results, the primary conclusion is that data corresponding to different water
 514 levels at the toe of the structure do not converge into a single formula and exhibit high
 515 uncertainty when $c_{VG}=1.75$ is applied uniformly for all data. Therefore, Eq. 3 can be
 516 adjusted to account for the effects of shallow water conditions. **Figure 11** shows that the
 517 recalibrated van Gent formula exhibits a better agreement with the experimental data if
 518 different water levels are considered separately. In this context, the influence of the
 519 spectral wave period becomes evident.

520 Based on these findings, a new formula is developed to fit the new experimental dataset
 521 and provide better insights into the effects of shallow water. Eq. 3 was modified by adding
 522 the influence of the spectral wave steepness (wave period) computed at the toe of the
 523 structure as a function of H_{m0} . All incident wave parameters were computed at the toe of
 524 the structure and $s_{m-1,0}$ was calculated using the deep water wavelength formula,
 525 considering the incident wave parameters at the toe of the breakwater. Results are
 526 reported in **Figure 12** and demonstrate that the modified formula (Eq. 7), provides a better
 527 prediction of the observed damage for the new dataset if a regression coefficient $c_{VG,new}$

528 equal to 3.3 is used, across the different shallowness conditions investigated in the present
 529 study.

$$\frac{H_{m0}}{\Delta D_{n50}} = c_{VG,new} \sqrt{\cot \alpha} \left(1 + \frac{D_{n50,core}}{D_{n50}} \right) s_{m-1,0}^{0.1} \left(\frac{S}{\sqrt{N_w}} \right)^{\frac{1}{5}} \quad \text{Eq. 7}$$

530



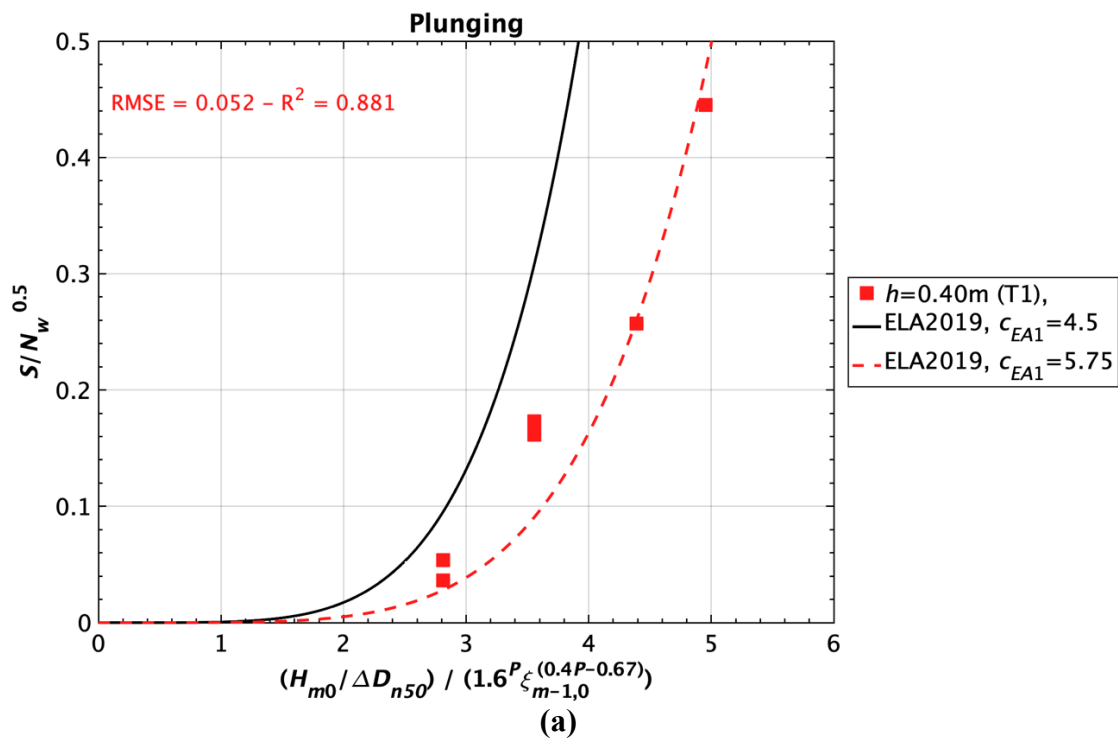
531 **Figure 12.** Refitting of the simple formula of van Gent et al. (2003) according to Eq. 7.

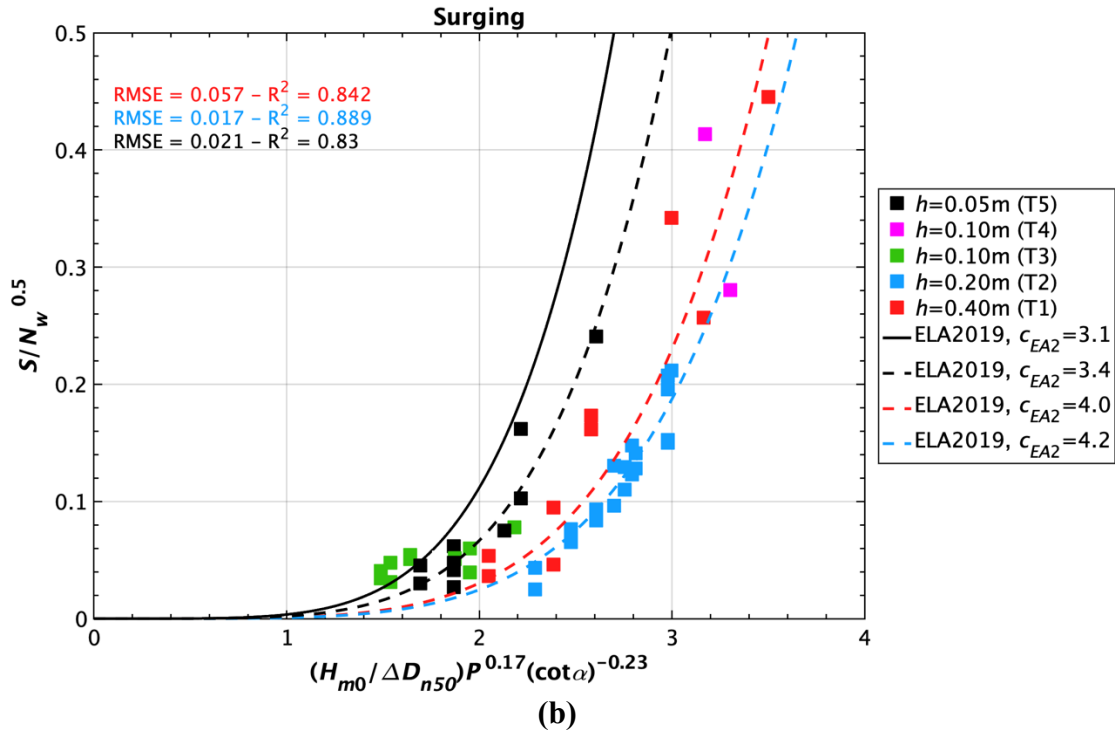
532 *5.2.2 Eldrup and Andersen (2019)*

533 **Figure 13** presents the new data plotted alongside the stability formulae proposed by
 534 Eldrup and Andersen (2019) (EA, Eq. 4). For each breakwater configuration, the
 535 permeability factor P , reported in **Table 3**, was estimated based on the method proposed
 536 by Eldrup et al. (2019).

537 Results show that only a few tests in intermediate waters experience plunging breaking
 538 waves on the structure (**Figure 13a**), whereas all the other data experienced surging
 539 breaking conditions (**Figure 13b**). The observed dimensionless damages are calculated
 540 using Eqs. 4a and 4b, shown in **Figures 13a** and **13b**, respectively, where the black solid

541 curves represent the theoretical predicted damage, with a regression coefficient c_{EA1} equal
 542 to 4.5 in plunging breaking conditions and c_{EA2} equal to 3.1 in surging ones. Results reveal
 543 that, in both breaking conditions, the predictions generally overestimate the observed
 544 damage, and such a difference increases as the damage level increases. In surging
 545 conditions, the empirical equation aligns better with the observed low damage values in
 546 very and extremely shallow water conditions (black and green squares), even if the bias
 547 increases in extremely shallow water when the structure is subjected to higher damage
 548 levels. In all other conditions, the predicted damage is overestimated. In both graphs, the
 549 recalibrated regression lines based on the newly acquired data are shown, showing a better
 550 fit with a regression coefficient c_{EA1} equal to 5.75 for plunging conditions in intermediate
 551 waters, and c_{EA2} equal to 3.4, 4.0 and 4.2 for very shallow, intermediate and shallow
 552 conditions, respectively.





553 **Figure 13.** Refitting of the Eldrup and Andersen (2019) stability formula for different
 554 shallowness conditions: a) plunging waves; b) surging waves.

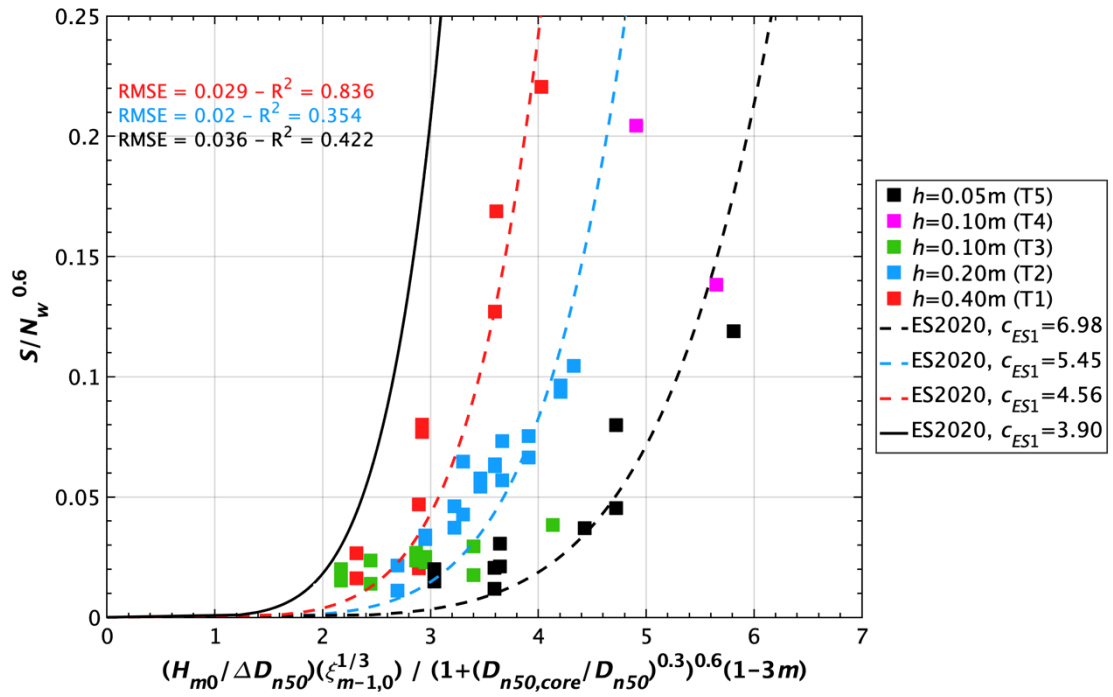
555 *5.2.3 Etemad-Shahidi et al. (2020)*

556 A similar comparison was also conducted using the stability formula proposed by
 557 Etemad-Shahidi et al. (2020) (ES, Eq. 5). **Figure 14** reports the new data plotted
 558 according to Eq. 5b, namely for surging conditions, since $\zeta_{m-1,0,t} \geq 1.8$ is observed for the
 559 entire dataset. Also in this case, the primary conclusion remains that new data, referring
 560 to different water levels, do not tend to collapse into a single cluster and are overestimated
 561 by the original formula with a regression coefficient c_{ES2} equal to 3.9. Experimental data
 562 under intermediate conditions show less deviation from predictions compared to other
 563 shallowness conditions. Thus, data were grouped by water levels, and the new regression
 564 coefficients were determined for the original equation. Specifically, results demonstrate
 565 a good estimation of damage for deep, shallow, and very and extremely shallow water
 566 conditions with $c_{ES2}=4.56$ (dotted red line), $c_{ES2}=5.45$ (dotted blue line), and $c_{ES2}=6.98$
 567 (dotted black line), respectively. In this last case, very shallow ($h=0.10$ m) and extremely

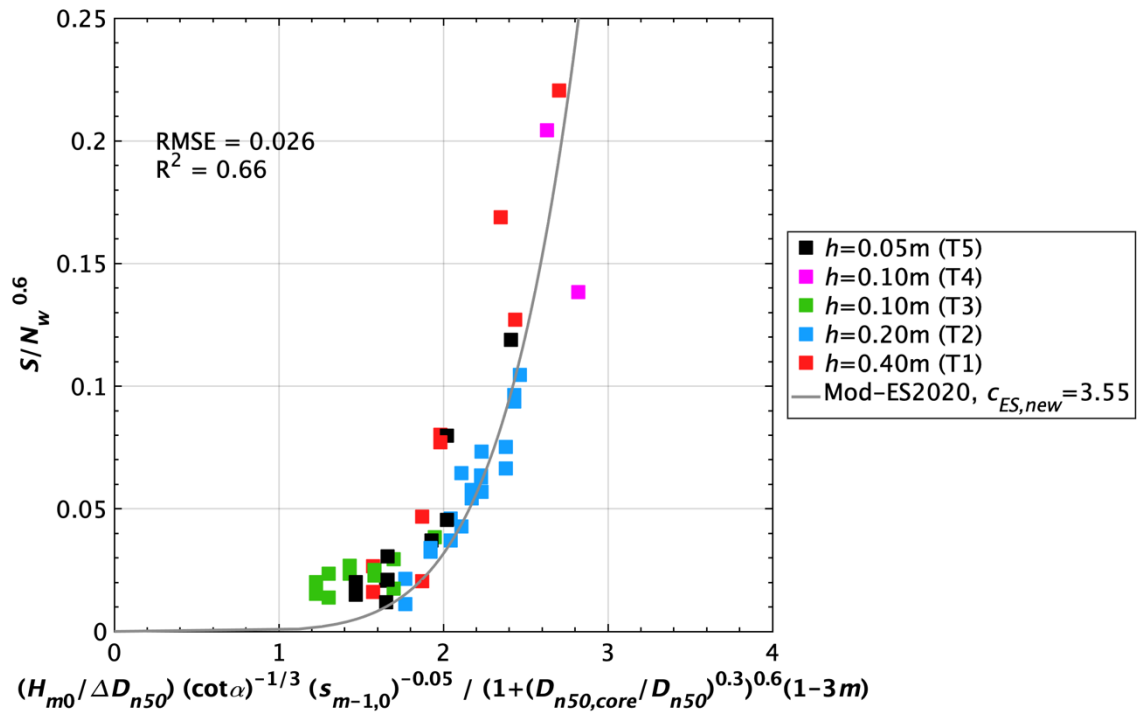
568 shallow ($h=0.05$ m) conditions exhibit the same behaviour and were aggregated. As with
 569 the VG equation, the effect of the spectral wave steepness was incorporated into the
 570 formulation, specifically aimed to fit the new experimental dataset, as reported in Eq. 8:

$$\frac{H_{m0}}{\Delta D_{n50}} = c_{ES,new} C_p N_w^{-\frac{1}{10}} \cot \alpha^{\frac{1}{3}} S_{m-1,0}^{\frac{1}{6}} s_{m-1,0}^{\frac{1}{20}} \quad \text{surge if } \xi_{m-1,0} \geq 1.8 \quad \text{Eq. 8}$$

571 Results shown in **Figure 15** demonstrate that incorporating the spectral wave steepness
 572 into the model leads to a good correlation between the data and the expression for all
 573 conditions with $c_{ES,new}=3.55$ (Eq. 8). In the original formulation, the spectral wave
 574 steepness is explicitly incorporated within the surf similarity parameter. In this approach,
 575 the structure slope and wave steepness are treated as separate variables, as the surf
 576 similarity parameter may not be the most effective parameter for characterising both
 577 influences simultaneously. This new formulation was necessary, particularly under
 578 shallow water conditions, to recalculate both the regression coefficient $c_{ES,new}$ and the
 579 power exponent of the wave steepness, which was observed to differ from the exponent
 580 of the surf similarity parameter. As for the VG formulation, the wave steepness power
 581 was incorporated into the ES equations by first establishing its physical influence, given
 582 the direct proportionality of the stability number (N_s) to wave steepness ($s_{m-1,0}$), and then
 583 calibrating the optimal exponent to fit the new experimental data.



584 **Figure 14.** Refitting of the Etemad-Shahidi et al. (2020) stability formula with the new
 585 data.



586 **Figure 15.** Refitting of the Etemad-Shahidi et al. (2020) stability formula according to
 587 Eq. 8.

588 **6. Conclusions and future perspectives**

589 Rock armour stability has been studied using physical model experiments with rubble
590 mound breakwaters in shallow water with various hydrodynamic conditions with severe
591 wave breaking along a 1V:30H foreshore. Four distinct breakwater configurations and
592 water levels were tested, ranging from deep to extremely shallow foreshores, for a total
593 of 33 tests. The aim was to investigate the influence of very and extremely shallow water
594 conditions (h_r up to 5), which have hardly been tested systematically before. The
595 experimental results were utilised to assess the performance of existing stability formulae
596 specifically designed for such conditions, namely those proposed by van Gent et al.
597 (2003) (VG), Eldrup and Andersen (2019) (EA), and Etemad-Shahidi et al. (2020) (ES)
598 using the newly obtained data. Initially, the accuracy of the original formulae was tested
599 against the experimental findings, highlighting discrepancies in their performance. To
600 address these issues, the formulae were recalibrated grouping the data based on water
601 levels, and new regression coefficients were derived to better fit the new experimental
602 data. Additionally, modified versions of the VG and ES formulae were developed to
603 account for the effects of incident wave steepness, improving their ability to reflect
604 shallow water dynamics.

605 The application of the original formulation by VG to the new data reveals that data
606 pertaining to different water levels at the toe of the structure do not converge into a single
607 formula and exhibit significant uncertainty when a unique coefficient ($c_{VG}=1.75$) is
608 applied. While a reliable estimation of damage for very shallow water was noted, there
609 was an overestimation of the predicted damage for intermediate and shallow water, and
610 an underestimation in extremely shallow water. This means that the influence of shallow
611 water is not properly incorporated in the stability equation. Therefore, for each water

612 level, the formula was recalibrated to derive new regression coefficients c_{VG} , depending
613 on water levels, showing that data in intermediate and shallow water exhibited similar
614 behaviour ($c_{VG}=2.3$), whereas data in extremely shallow water were well predicted if a
615 regression coefficient $c_{VG}=1.5$ was used. For our dataset, a more accurate prediction of
616 the observed damage was achieved if the influence of the incident wave steepness was
617 considered. Indeed, a new equation (Eq. 7) was derived specifically valid in shallow water
618 with $c_{VG,new}=3.3$.

619 Discrepancies between observed and predicted damage were noted also for the formulae
620 proposed by Eldrup and Andersen (2019) and Etemad-Shahidi et al. (2020). For EA
621 formulation, the comparison among predicted and observed damage measurements
622 showed that, in both surging and plunging breaking conditions, the predictions generally
623 tended to overestimate the observed damage as the damage level increases. Under surging
624 conditions, the observed damage was more accurately predicted especially for low S-
625 values in very and extremely shallow water. The bias grew in extremely shallow water
626 when the structure experienced higher damage levels. The recalibration of the formula,
627 based on the new acquired data, showed a better fit with a regression coefficient $c_{EA1}=5.75$
628 for plunging conditions in intermediate waters, and c_{EA2} equal to 3.4, 4.0 and 4.2 for very
629 shallow, intermediate and shallow conditions, respectively.

630 The stability formula proposed by Etemad-Shahidi et al. (2020) (Eq. 5), applied to surging
631 conditions for the entire dataset, showed that the main finding remained consistent. The
632 new data, corresponding to different water levels, did not converge into a single cluster
633 and were generally overestimated. In intermediate conditions, a lower bias was observed
634 compared to the other water levels. Consequently, new regression coefficients were
635 calculated, providing accurate damage estimates for deep, shallow, very/extremely
636 shallow conditions with coefficients c_{ES2} equal to 4.56, 5.45, and 6.98, respectively. As

637 with VG equation, the impact of wave steepness was integrated into the formula (Eq. 8),
638 resulting in a good prediction of the new data with $c_{ES,new}=3.55$. In this context, the
639 structure slope and wave steepness were treated as separate variables, as the surf
640 similarity parameter may not be the most effective parameter for characterising both
641 influences simultaneously.

642 It is important to emphasise that the dataset used in this study is relatively small and is
643 closely tied to particular wave conditions and structural layouts. This limitation poses
644 challenges when attempting to generalise the derived equations to broader contexts.
645 Consequently, further experiments are necessary, particularly under very shallow and
646 extremely shallow water conditions, while also accounting for varying foreshore and
647 structure slopes. This will allow for a more comprehensive evaluation of the proposed
648 formulae, ultimately enhancing their utility and reinforcing their applicability in real-
649 world engineering applications.

650 **Credit authorship contribution statement**

651 All the authors contributed in equal measure to all states of the development and
652 production of this paper. All authors read and agreed to the published version of the
653 manuscript.

654 **Declaration of competing interest**

655 The authors declare that they have no known competing financial interests or personal
656 relationships that could have appeared to influence the work reported in this paper.

657 **Data availability**

658 Data will be made available on request.

659 **Acknowledgments**

660 This work was funded by Piano Nazionale di Ripresa e Resilienza (PNRR), Missione 4
661 *Istruzione e Ricerca*, Componente C2, Investimento 1.1 *Fondo per il Programma*
662 *Nazionale di Ricerca e Progetti di Rilevante Interesse Nazionale (PRIN)*, Research
663 project *A PRObabilistic fraMEwork for coasTal and harbor dEfense in the cOntext of*
664 *climate change, PROMETEO (P20224T9SK)*

665 **References**

- 666 Ahrens, J. P., 1970. The influence of breaker type on riprap stability. *Coastal Engineering*
667 *Proceedings 1970*.
- 668 Ahrens, J. P., & McCartney, B. L., 1975. *Wave period effect on the stability of riprap*.
- 669 Allsop, N. W. H., Durand, N., & Hurdle, D. P., 1999. Influence of steep seabed slopes on
670 breaking waves for structure design. *Coastal Engineering Proceedings 1998*. 906-
671 919. <https://doi.org/10.1061/9780784404119.067>
- 672 Allsop, N. W. H., 2021. Old British breakwaters: how have engineering developments
673 influenced their survival? *Doctoral dissertation*, University of Edinburgh.
- 674 Altomare, C., Suzuki, T., Chen, X., Verwaest, T., & Kortenhaus, A., 2016. Wave
675 overtopping of sea dikes with very shallow foreshores. *Coastal Engineering*, 116,
676 236-257. <https://doi.org/10.1016/j.coastaleng.2016.07.002>
- 677 Altomare, C., Suzuki, T., & Verwaest, T., 2020. Influence of directional spreading on
678 wave overtopping of sea dikes with gentle and shallow foreshores. *Coastal*
679 *Engineering*, 157, 103654. <https://doi.org/10.1016/j.coastaleng.2020.103654>
- 680 Atkinson, A., & Baldock, T. E., 2016. A high-resolution sub-aerial and sub-aqueous laser
681 based laboratory beach profile measurement system. *Coastal Engineering*, 107,
682 28-33. <https://doi.org/https://doi.org/10.1016/j.coastaleng.2015.10.005>
- 683 Booij, N., Ris, R. C., & Holthuijsen, L. H., 1999. A third-generation wave model for
684 coastal regions: 1. Model description and validation. *Journal of Geophysical*
685 *Research: Oceans*, 104(C4), 7649-7666.
686 <https://doi.org/https://doi.org/10.1029/98JC02622>
- 687 Bradbury, A., Allsop, W., Latham, J.-P., Mannion, M., & Poole, A., 1988. Rock armour
688 for rubble mound breawaters, sea walls, and revetments: recent progress. H. R.
689 Wallingford.
- 690 Brancasi, A., Leone, E., Francone, A., Scaravaglione, G., & Tomasicchio, G. R., 2022.
691 On formulae for wave transmission at submerged and low-crested breakwaters.
692 *Journal of Marine Science and Engineering*, 10(12), 1986.
693 <https://doi.org/https://doi.org/10.3390/jmse10121986>
- 694 Broderick, L. L., & Ahrens, J. P., 1982. Riprap stability scale effects. C. E. R. C. (CERC).
- 695 Burcharth, H. F., Andersen, T. L., & Lara, J. L., 2014. Upgrade of coastal defence
696 structures against increased loadings caused by climate change: A first
697 methodological approach. *Coastal Engineering*, 87, 112-121.
698 <https://doi.org/10.1016/j.coastaleng.2013.12.006>
- 699 Calabrese, M., Buccino, M., Ciardulli, F., Di Pace, P., Tomasicchio, G. R., & Vicinanza,
700 D., 2011. Wave run-up and reflection at rubble mound breakwaters with

701 Ecopodetm armor layer. *Coastal Engineering Proceedings* 2011.
702 <http://dx.doi.org/10.9753/icce.v32.structures.45>

703 Campos, Á., Castillo, C., & Molina-Sanchez, R., 2020. Damage in rubble mound
704 breakwaters. Part I: Historical review of damage models. *Journal of Marine*
705 *Science and Engineering*, 8(5), 317.
706 <https://doi.org/https://doi.org/10.3390/jmse8050317>

707 Campos, Á., Molina-Sanchez, R., & Castillo, C., 2020. Damage in rubble mound
708 breakwaters. Part II: Review of the definition, parameterization, and measurement
709 of damage. *Journal of Marine Science and Engineering*, 8(5), 306.
710 <https://doi.org/https://doi.org/10.3390/jmse8050306>

711 Ciardulli, F., Cuomo, G., Buccino, M., & Calabrese, M., 2013. Experimental and
712 numerical investigation on wave transmission past rubble-mound submerged
713 breakwaters. From Sea to Shore—Meeting the Challenges of the Sea. *Coasts,*
714 *Marine Structures and Breakwaters 2013*.

715 CIRIA/CUR/CETMEF, 2007. The Rock Manual. The Use of Rock in Hydraulic
716 Engineering. CIRIA.

717 Díaz-Carrasco, P., Molines, J., Gómez-Martín, M. E., & Medina, J. R., 2023. Simple and
718 explicit neural network-derived formula to estimate wave reflection on mound
719 breakwaters. *Coastal Engineering*, 186, 104404.
720 <https://doi.org/http://dx.doi.org/10.1016/j.coastaleng.2023.104404>

721 Eldrup, M. R., & Andersen, T. L., 2019. Extension of shallow water rock armour stability
722 formulae to nonlinear waves. *Coastal Engineering*, 153, 103536.
723 <https://doi.org/https://doi.org/10.1016/j.coastaleng.2019.103536>

724 Eldrup, M. R., Lykke Andersen, T., & Burcharth, H. F., 2019. Stability of rubble mound
725 breakwaters—A study of the notional permeability factor, based on physical
726 model tests. *Water*, 11(5), 934. <https://doi.org/10.3390/w11050934>

727 Eldrup, M. R., & Andersen, T. L., 2024. Generation Of Highly Nonlinear Waves In A
728 Short Wave Flume. CoastLab Proceedings 2024: Physical Modelling in Coastal
729 Engineering and Science. DOI: [10.59490/coastlab.2024.687](https://doi.org/10.59490/coastlab.2024.687)

730 Etemad-Shahidi, A., Bali, M., & van Gent, M. R. A., 2020. On the stability of rock
731 armored rubble mound structures. *Coastal Engineering*, 158, 103655.
732 <https://doi.org/https://doi.org/10.1016/j.coastaleng.2020.103655>

733 Frostick, L. E., McLelland, S. J., & Mercer, T. G., 2011. Users guide to physical
734 modelling and experimentation. IAHR Des. Manual.

735 Goda, Y., 2010. Random seas and design of maritime structures. World scientific.

736 Goda, Y., 2010. Reanalysis of regular and random breaking wave statistics. *Coastal*
737 *Engineering Journal*, 52(1), 71-106.
738 <https://doi.org/10.1142/S0578563410002129>

739 Goda, Y., 2012. Design wave height selection in intermediate-depth waters. *Coastal*
740 *engineering*, 66, 3-7.

741 Herrera, M. P., & Medina, J. R., 2015. Toe berm design for very shallow water on steep
742 sea bottoms. *Coastal Engineering*, 103, 67-77.
743 <https://doi.org/10.1016/j.coastaleng.2015.06.005>

744 Herrera, M. P., Gomez-Martín, M. E., & Medina, J. R., 2017. Hydraulic stability of rock
745 armors in breaking wave conditions. *Coastal Engineering*, 127, 55-67.
746 <https://doi.org/https://doi.org/10.1016/j.coastaleng.2017.06.010>

747 Hofland, B., Chen, X., Altomare, C., & Oosterlo, P., 2017. Prediction formula for the
748 spectral wave period $T_{m-1,0}$ on mildly sloping shallow foreshores. *Coastal*
749 *Engineering*, 123, 21-28.
750 <https://doi.org/https://doi.org/10.1016/j.coastaleng.2017.02.005>

- 751 Hudson, R. Y., 1975. Reliability of rubble-mound breakwater stability models. US Army
752 Engineer Waterways Experiment Station.
- 753 Hudson, R. Y., 1959. Laboratory investigation of rubble-mound breakwaters. *Journal of*
754 *the waterways and Harbors division*, 85(3), 93-121.
- 755 Hughes, S. A., 1993. Physical models and laboratory techniques in coastal engineering
756 (Vol. 7). World Scientific. <https://doi.org/https://doi.org/10.1142/2154>
- 757 Iribarren, R., 1938. *Una Fórmula para el Cálculo de los Diques de Escollera*.
- 758 Kamphuis, J. W., 1996. Experiments on design wave height in shallow water. *Coastal*
759 *Engineering Proceedings 1996*. <https://doi.org/10.9753/icce.v25.%25p>
- 760 Lamberti, A., & Tomasicchio, G. R., 1997. Stone mobility and longshore transport at
761 reshaping breakwaters. *Coastal Engineering*, 29(3-4), 263-289.
762 [https://doi.org/https://doi.org/10.1016/S0378-3839\(96\)00027-0](https://doi.org/https://doi.org/10.1016/S0378-3839(96)00027-0)
- 763 Latham, J.-P., Mannion, M., Poole, A., Bradbury, A., & Allsop, N., 1988. The influence
764 of armourstone shape and rounding on the stability of breakwater armour layers.
765 Coastal engineering group report 1, Q. M. College.
- 766 Losada, M. Á., 2021. Method to assess the interplay of slope, relative water depth, wave
767 steepness, and sea state persistence in the progression of damage to the rock layer
768 over impermeable dikes. *Ocean Engineering*, 239, 109904.
769 <https://doi.org/https://doi.org/10.1016/j.oceaneng.2021.109904>
- 770 Losada, M. A., & Gimenez-Curto, L. A., 1979. The joint effect of the wave height and
771 period on the stability of rubble mound breakwaters using Iribarren's number.
772 *Coastal Engineering*, 3, 77-96. [https://doi.org/https://doi.org/10.1016/0378-](https://doi.org/https://doi.org/10.1016/0378-3839(79)90011-5)
773 [3839\(79\)90011-5](https://doi.org/https://doi.org/10.1016/0378-3839(79)90011-5)
- 774 Lykke Andersen, T., & Eldrup, M. R., 2024. Applicability of Reflection Separation
775 Algorithms to Nonlinear Irregular Waves over Sloping Foreshores. In *CoastLab*
776 *2024: Physical Modelling in Coastal Engineering and Science* TU Delft Open.
777 <https://doi.org/10.59490/coastlab.2024.685>
- 778 Mansard, E. P. D., & Funke, E. R., 1980. The measurement of incident and reflected
779 spectra using a least squares method. *Coastal Engineering Proceedings 1980*.
780 <https://doi.org/10.9753/icce.v17.8>
- 781 Mares-Nasarre, P., van Gent, M. R. A., & Morales-Nápoles, O., 2024. A copula-based
782 model to describe the uncertainty of overtopping variables on mound breakwaters.
783 *Coastal Engineering*, 189, 104483.
784 <https://doi.org/https://doi.org/10.1016/j.coastaleng.2024.104483>
- 785 Marino, S., Scaravaglione, G., Francone, A., Valentini, N., Saponieri, A., Damiani, L.,
786 van Gent, M.R.A. & Tomasicchio, G., 2022. Laboratory investigation on armour
787 stability for extremely shallow water conditions. Proceedings of the IAHR World
788 Congress. Proceedings of the 39th IAHR World Congress. Pages 5973 - 5979,
789 Code 299039, 2022, <http://dx.doi.org/10.3850/iahr-39wc2521711920221364>
- 790 Marino, S., Galantucci, R. A., & Saponieri, A., 2023. Measuring rock slope damage on
791 rubble mound breakwater through digital photogrammetry. *Measurement*, 211,
792 112656. <https://doi.org/https://doi.org/10.1016/j.measurement.2023.112656>
- 793 Melby, J. A., & Hughes, S. A., 2003. Armor stability based on wave momentum flux.
794 *Coastal Structures 2003, Reston, VA*. [https://doi.org/10.1061/40733\(147\)5](https://doi.org/10.1061/40733(147)5)
- 795 Melby, J. A., & Kobayashi, N., 1999. Damage progression and variability on breakwater
796 trunks. *Coastal Structures 1999*.
- 797 Melby, J. A., & Kobayashi, N., 2011. Stone armor damage initiation and progression
798 based on the maximum wave momentum flux. *Journal of Coastal Research*,
799 27(1), 110-119.

800 Melby, J. A., Massey, T. C., Stehno, A. L., Nadal-Caraballo, N. C., Misra, S., Gonzalez,
801 V. M., & Engineer Research and Development Center (US), 2021. Sabine Pass to
802 Galveston Bay, TX Pre-construction, Engineering and Design (PED): Coastal
803 storm surge and wave hazard assessment: Report 1—Background and approach.
804 Vicksburg, MS: US Army Engineer Research and Development Center, Coastal
805 and Hydraulics Laboratory.

806 Scaravaglione, G., Latham, J.-P., Xiang, J., Francone, A., & Tomasicchio, G. R., 2022.
807 Historical overview of the structural integrity of Concrete Armour Units. *Coastal
808 and Offshore Science and Engineering*, 1, 68-98.
809 https://doi.org/https://doi.org/10.53256/COSE_220105

810 Scaravaglione, G., Marino, S., Francone, A., Damiani, L., Tomasicchio, G. R., &
811 Saponieri, A., 2024. Laboratory investigation on pore pressures inside a rubble
812 mound breakwater in depth-limited waters. *Applied Ocean Research*, 147,
813 103988. <https://doi.org/https://doi.org/10.1016/j.apor.2024.103988>

814 Shah, A. M., & Kamphuis, J. W., 1996. The swash zone: a focus on low frequency
815 motion. *Coastal Engineering Proceedings 1996*.

816 Smith, G., Wallast, I., & van Gent, M. R. A., 2002. Rock slope stability with shallow
817 foreshores. *Coastal Engineering Proceedings 2002*.
818 https://doi.org/10.1142/9789812791306_0128

819 Thompson, D. M., & Shuttler, R. M., 1975. Riprap design for wind-wave attack, a
820 laboratory study in random waves. Wallingford report EX707 for CIRIA, H. R.
821 Wallingford.

822 U. S. A. C. E., 2002. CEM: Coastal Engineering Manual. U.S. Army Corps of Engineers.
823 https://books.google.com/books?id=QLO_jwEACAAJ

824 Van der Meer, J. W., 1988. Rock slopes and gravel beaches under wave attack. *Ph.D.
825 Thesis*, Delft Hydraulics.

826 Van der Meer, J. W., 2021. Rock armour slope stability under wave attack; the Van der
827 Meer Formula revisited. *Journal of Coastal and Hydraulic Structures*, 1.
828 <https://doi.org/https://doi.org/10.48438/jchs.2021.0008>

829 Van Gent, M.R.A., 1999. Physical model investigations on coastal structures with
830 shallow foreshores; 2D model tests with single and double-peaked wave energy
831 spectra, Delft Hydraulics Report H3608, December 1999, Delft.

832 Van Gent, M. R. A., 2001. Wave runup on dikes with shallow foreshores. *Journal of
833 Waterway, Port, Coastal, and Ocean Engineering*, 127(5), 254-262.
834 [https://doi.org/http://dx.doi.org/10.1061/\(ASCE\)0733-950X\(2001\)127:5\(254\)](https://doi.org/http://dx.doi.org/10.1061/(ASCE)0733-950X(2001)127:5(254))

835 Van Gent, M. R. A., 2004. On the stability of rock slopes. Environmentally Friendly
836 Coastal Protection: Proceedings of the NATO Advanced Research Workshop on
837 Environmentally Friendly Coastal Protection Structures Varna, Bulgaria.
838 http://dx.doi.org/10.1007/1-4020-3301-X_5

839 Van Gent, M. R. A., Smale, A. J., & Kuiper, C., 2003. Stability of rock slopes with
840 shallow foreshores. *Coastal Structures 2003*.
841 [http://dx.doi.org/10.1061/40733\(147\)9](http://dx.doi.org/10.1061/40733(147)9)

842 Van Gent, M. R. A., & Teng, D. Y. Y., 2023. Climate adaptation of coastal structures:
843 Application of adaptation pathways for rubble mound breakwaters. *PIANC-
844 COPEDEC 2023, Manila, Philippines*.

845 Vidal, C., Medina, R., & Lomónaco, P., 2006. Wave height parameter for damage
846 description of rubble-mound breakwaters. *Coastal Engineering*, 53(9), 711-722.
847 <https://doi.org/https://doi.org/10.1016/j.coastaleng.2006.02.007>

848 Wolters, G., van Gent, M.R.A., Allsop, W., Hamm, L., & Mühlestein, D., 2009.
849 HYDRALAB III: Guidelines for physical model tests for rubble mound
850 breakwaters.,Coast, Marine Structures and Breakwaters 2009, Edinburgh.
851 Wolters, G., van Gent, M.R.A. Hofland, B. & Wellens, P., 2014. Wave damping and
852 permeability scaling in rubble mound breakwaters, Proc. Coastlab 2014, Varna.
853 Zelt, J. A., & Skjelbreia, J. E., 1992. Estimating incident and reflected wave fields using
854 an arbitrary number of wave gauges. *Coastal Engineering Proceedings 1992*,
855 1(23), 777-789. <https://doi.org/10.9753/icce.v23.%25p>
856

857 **Glossary Name Symbol Unit**

Name	Symbol	Unit
Structure seaward slope angle	α	[°]
Spectrum enhancement factor	γ	[-]
Relative buoyant density of the rock armour	Δ	[-]
Surf similarity parameter using H_{m0} and T_m	ξ_m	[-]
Surf similarity parameter using H_{m0} and $T_{m-1,0}$	$\xi_{m-1,0}$	[-]
Transition surf similarity parameter in EA formula	$\xi_{m-1,0,c}$	[-]
Surf similarity parameter using H_s and $T_{m-1,0}$	$\xi_{s-1,0}$	[-]
Transition surf similarity parameter	$\xi_{s-1,0,c}$	[-]
Nonlinearity parameter	Π_0	[-]
Density of the armour rock	ρ_r	[Kg/m ³]
Density of the water	ρ_w	[Kg/m ³]
Eroded area	A_e	[m ²]
Accretion area	A_a	[m ²]
Regression fitting parameters	$a, b,$	[-]
Blockiness coefficient	BLc	[%]
Regression fitting coefficients for the stability equations	$CVG, CVG_{new},$ $CEA1, CEA2,$ $CES1, CES2,$ CES_{new}	[-]
Stone shape coefficients	c_{pl}, c_{su}	[-]
Permeability coefficient, $C_p = \left[1 + \left(\frac{D_{n50,core}}{D_{n50}} \right)^{3/10} \right]^{3/5}$	C_p	[-]
Grading uniformity coefficient	D_{85}/D_{15}	[-]
Mass exceeded by 85% of a sample by weight	D_{85}	[m]
Mass exceeded by 15% of a sample by weight	D_{15}	[m]
Armour nominal median stone diameter, $D_{n50} = (M_{50}/\rho_r)^{1/3}$	D_{n50}	[m]
Core nominal median stone diameter	$D_{n50,core}$	[m]
Underlayer nominal median stone diameter	$D_{n50,underlayer}$	[m]

Spatial evolution of slope elevation changes with respect to the initial slope	dz	[m]
Gravity acceleration	g	[m/s ²]
Water depth at toe of the structure	h	[m]
Relative water depth, $h_r=H_{m0,o}/h$	h_r	[-]
Water depth at the end of the transitional slope	h_t	[m]
Significant wave height in the time domain, $H_s=H_{1/3}$	H_s	[m]
Significant (spectral) wave height in frequency domain, $H_{m0}=4(m_0)^{1/2}$	H_{m0}	[m]
Wave height exceeded by 2 percent of the waves in time domain	$H_{2\%}$	[m]
Average wave height of the 50 highest waves in the time domain	$H_{1/50}$	[m]
Wavelength using T_m	L_m	[m]
Wavelength using $T_{m-1,0}$	$L_{m-1,0}$	[m]
Wavelength using T_p	L_p	[m]
Length-to-thickness ratio	LT	[-]
Foreshore slope angle	m	[°]
Zero th moment of the frequency spectrum	m_0	[m ²]
Infragravity (IG) zero th moment of the frequency spectrum	m^{IG}_0	[m ²]
Total zero th moment of the frequency spectrum	m^{TOT}_0	[m ²]
Median mass of the armour rock grading	M_{50}	[Kg]
Porosity of the structure core	n	[-]
Number of observations	N	[-]
Stability number	N_s	[-]
Number of waves	N_w	[-]
Notional permeability factor	P	[-]
Reynolds number at the armour layer	Re_A	[-]
Reynolds number inside the structure core	Re_p	[-]
Crest freeboard above the still water level	R_c	[m]
Root Mean Square Error	$RMSE$	[-]
Determination coefficient	R^2	[-]
Damage level	S	[-]
Wave steepness using H_{m0} and T_m	s_m	[-]
Wave steepness using H_{m0} and $T_{m-1,0}$	$s_{m-1,0}$	[-]
Negative spectral energy wave period, $T_{m-1,0}=m_{-1}/m_0$	$T_{m-1,0}$	[s]
Mean period	T_m	[s]

Peak wave period	T_p	[s]
Duration of the test	t_r	[s]
Longitudinal coordinate positive towards the external side of the structure	x	[m]
Transversal coordinate positive in the wave propagation direction	y	[m]
Vertical coordinate positive in the upper direction	z	[m]

858